Aerosol modeling for regional climate studies: Application to anthropogenic particles and evaluation over a European/African domain

Fabien Solmon, Filippo Giorgi, Cathy Liousse

Aerosol modelling for regional climate studies: application to anthropogenic particles and evaluation over a European/African domain

By F. SOLMON[1]*, F. GIORGI[1] and C. LIOUSSE[2], [1]*Abdus Salam International Center for theoretical Physics, Strada Costiera 11, 34100 Trieste, Italy;* [2]*Laboratoire d'aérologie, 16 avenue Edouard Belin, 34100 Toulouse, France*

ABSTRACT

A simplified anthropogenic aerosol model for use in climate studies is developed and implemented within the regional climate model RegCM. The model includes sulphur dioxide, sulphate, hydrophobic and hydrophilic black carbon (BC) and organic carbon (OC) and is run for the winter and summer seasons of 2000 over a large domain extending from northern Europe to south tropical Africa. An evaluation of the model performance is carried out in terms of surface concentrations and aerosol optical depths (AODs). For sulphur dioxide and sulphate concentration, comparison of simulated fields and experimental data collected over the EMEP European network shows that the model generally reproduces the observed spatial patterns of near-surface sulphate. Sulphate concentrations are within a factor of 2 of observations in 34% (JJA) to 57% (DJF) of cases. For OC and BC, simulated concentrations are compared to different datasets. The simulated and observed values agree within a factor of 2 in 56% (DJF) to 62% (JJA) of cases for BC and 33% (JJA) to 64% (DJF) for OC. Simulated AODs are compared with ground-based (AERONET) and satellite (MODIS, MISR, TOMS) AOD datasets. Simulated AODs are in the range of AERONET and MISR data over northern Europe, and AOD spatial patterns show consistency with MODIS and TOMS retrievals both over Europe and Africa. The main model deficiencies we find are: (i) an underestimation of surface concentrations of sulphate and OC during the summer and especially over the Mediterranean region and (ii) a general underestimation of AOD, most pronounced over the Mediterranean basin. The primary factors we identify as contributing to these biases are the lack of natural aerosols (in particular, desert dust, secondary biogenic aerosols and nitrates), uncertainties in the emission inventories and aerosol cycling by moist convection. Also, in view of the availability of better observing datasets (e.g. as part of the AMMA project), we are currently working on improving these aspects of the model before applying it to climate studies. Despite the deficiencies identified above, we assess that our model shows a performance in line with that other coupled climate/aerosol models and can presently provide a useful tool for sensitivity and process studies.

1. Introduction

It is by now well established that atmospheric aerosols can have substantial climatic impacts through their direct and indirect effects (Haywood and Boucher, 2000; Penner et al., 2001; Cubasch et al., 2001). Aerosols are emitted via natural processes, such as desert dust lifting, sea spray, volcanic explosions or biogenic organic emissions, or result from anthropogenic activities, such as fossil fuel and biomass burning. Both natural and anthropogenic aerosols contribute to the climatic forcing, however the specific study of the anthropogenic component is crucial in view of assessing the impact of human activities on climate and air quality.

*Corresponding author.
e-mail: solmon@ictp.trieste.it

Aerosols of anthropogenic origin are mainly composed of sulphates (SO_4^{2-}), carbonaceous particles, typically divided in black carbon (BC) and organic carbon (OC), nitrates, ammonium and mineral dust of industrial origin. They are mostly emitted through fossil fuel combustion, biomass burning and industrial production. Being characterized by relatively short atmospheric life times, these compounds generally show highly spatial variability determined by local sources, rapid chemical transformations, transport and removal processes. As a result, the effects of anthropogenic aerosols are expected to be particularly relevant at the regional scale. For example, Giorgi et al. (2002, 2003) and Qian et al. (2003) assessed the regional climatic impacts deriving from the direct and indirect effects of anthropogenic aerosols over east Asia and found that these effects can contribute to explain a cooling trend observed over various regions of China

during the last decades of the 20th century. Ekman and Rodhe (2003) carried out a similar study for Europe and found that anthropogenic sulphate can induce a cooling of more than 1° over the region. As a final example, Menon et al. (2003) found substantial regional climatic effects induced by large BC aerosol forcing over south Asia.

Because the aerosol effects are especially important at the regional scale, the recent development of high-resolution regional climate models (RCMs) offers useful tools to assess the regional impacts of anthropogenic aerosols. Compared to global climate models (GCMs), the relatively high-resolution and detailed physical parametrizations offered by RCMs are particularly suitable to describe the complexity of aerosol processes.

The study of the climatic effects of aerosols requires the coupling of climate and chemistry/aerosol models. A number of detailed chemistry/aerosol schemes are today available, as used in chemistry transport models (CTMs) (e.g. Bessagnet et al., 2004) and for modelling pollution events (Seigneur, 2001). These schemes can include tens of species and hundreds of chemical reactions and therefore they are computationally very demanding. Because the study of aerosol climatic effects requires long simulations to extract the climate-impact signal from the underlying noise, the interactive coupling of complex climate models and CTMs is still computationally too expensive to allow many applications to climate-change studies, even when RCMs are used.

Alternatively, one can develop simplified chemistry modules of intermediate complexity for coupling to climate models. This has been done extensively for global modelling (e.g. Chin et al., 2002; Chung and Seinfeld, 2002; Reddy and Boucher, 2004), while fewer studies have coupled simplified aerosol models to RCMs (Qian et al., 2001; Giorgi et al., 2002, 2003; Tan et al., 2002; Ekman and Rodhe, 2003). Following these latter studies, here we develop a simplified aerosol model and implement it within the framework of the regional climate model RegCM (Giorgi and Mearns, 1999). The model is an extension of that of Qian et al. (2001) in that it includes, in addition to sulphate, anthropogenic OC and BC particles.

Our region of interest for the application of this new model configuration extends from Europe to sub-tropical African continent (to about 15° south). Besides offering large sulphur, OC and BC anthropogenic sources, this domain is characterized by contrasted climatic and chemical conditions and presents different sub-regions of interest: in high-emission areas, such as Europe, an accurate description of regional aerosol burdens and their chemical nature is still a key issue with regards to the effectiveness of emission reduction policies. West Africa represents a major region of aerosol source, where emissions, chemical and dynamical processes are still affected by large uncertainties (AMMA whitebook, 2001 http://medias.obs-mip.fr/amma/index.en.html). The Mediterranean basin shows a complex atmospheric chemistry influenced by regional emissions and long-range transport from both continental Europe and Africa (Lelieveld et al., 2002). Here, we test the model performance in simulating aerosol fields against station and remotely based observations for two opposite seasons.

We stress that this work is only the first step towards a more comprehensive development effort aimed at studying aerosol climatic effects on the European/African region. Although we include the dominant anthropogenic aerosol components, other aerosols are important in this region. Most noticeably, desert dust can provide an important aerosol loading and we are currently implementing a dust scheme in our model. However, the processes that regulate the emission of dust have quite different characteristics compared to those involved in the anthropogenic emissions, so that we will report on the dust scheme in a separate work. In addition, we do not include other natural biogenic emission and sea spray. Anthropogenic nitrate is also not included in this first approach. Finally, because our model does not include all major aerosol components (noticeably desert dust), we do not focus here on the climatic effect of aerosols, a topic which is left for later stages of more comprehensive model development.

2. Models, data and experiment design

2.1. Regional climate model and simulation domain

The RCM used in the present work is the Abdus Salam International Centre for Theoretical Physics (ICTP) RegCM (Giorgi et al., 1993a,b; Giorgi and Mearns, 1999; Pal et al., 2000). The RegCM is a hydrostatic, sigma vertical coordinate model whose dynamics is essentially the same as the hydrostatic version of the mesoscale model MM5 (Grell et al., 1994). Radiative transfer processes are from the NCAR global model CCM3 and are described by Kiehl et al. (1996). Land surface processes are described by the Biosphere–Atmosphere Transfer Scheme (BATS; Dickinson et al., 1993), while boundary layer processes follow the non-local parametrization of Holtslag et al. (1990). Finally, the scheme of Grell (1993) is used to describe moist convection and the parametrization of Pal et al. (2000) to represent non-convective precipitation. Over the years, the RegCM has been used for a wide range of applications, as described, for example by Giorgi and Mearns (1999).

The simulation domain encompasses most of Europe, the Mediterranean basin, the Sahara, Sahel and equatorial Africa with a 60-km spatial resolution and 18 vertical levels (Fig. 1). To assess seasonality effects, simulations are carried out for two opposite seasons: December 1999 through February 2000 and June through August 2000. The initial and lateral boundary conditions necessary to run the RegCM (Giorgi et al., 1993b) are obtained from re-analyses of observations from the National Center for Environmental Prediction (NCEP, Kalnay et al., 1996).

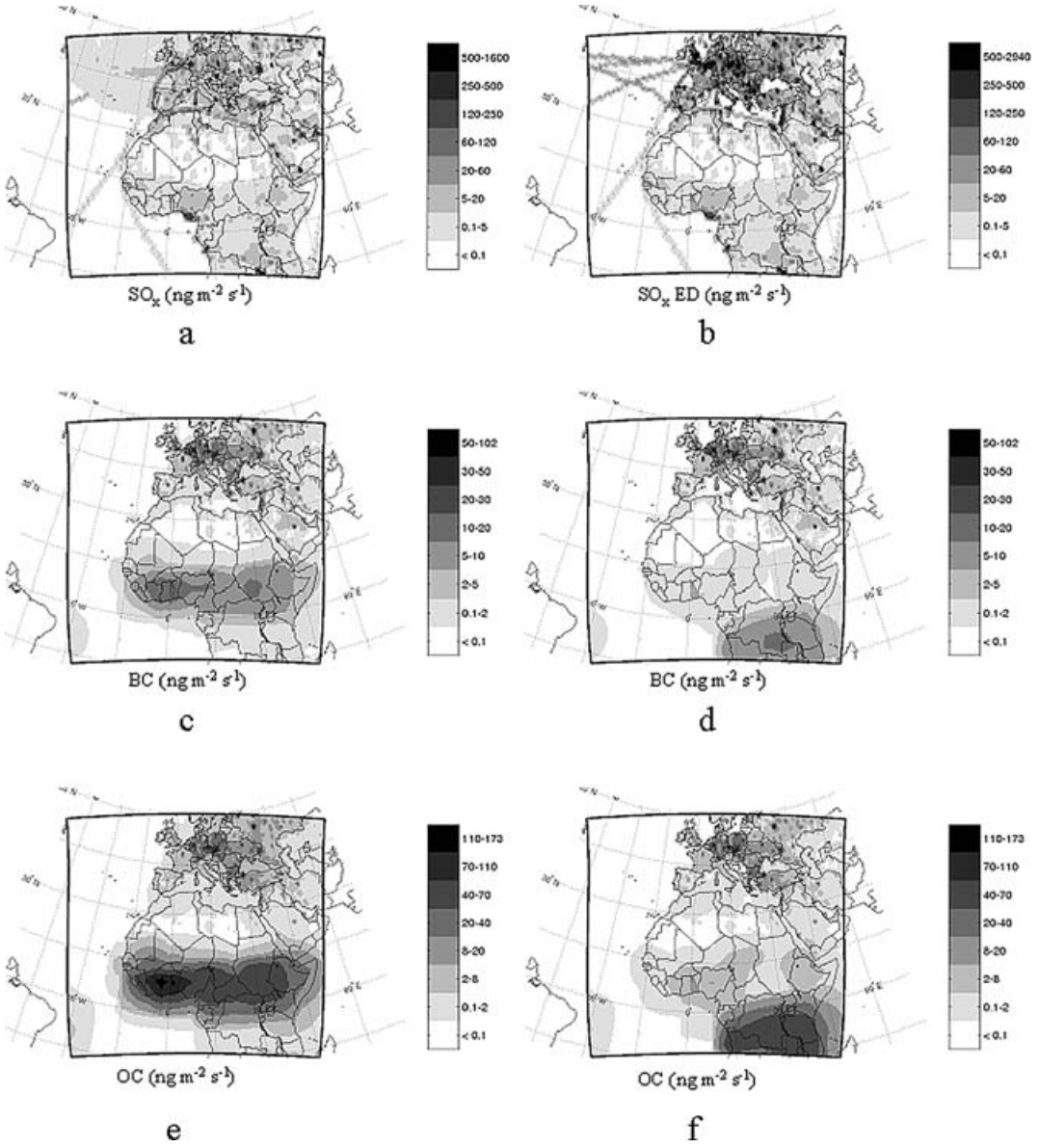

Fig 1. Primary emission fluxes (ng m^{-2} s^{-1}) over the domain of simulation: (a) SO_x based on the EMEP database over Europe and the EDGAR database elsewhere; (b) SO_x based on the EDGAR database over the whole domain (see text); (c) BC emission in January; (d) BC emission in July; (e) OC emission in January; (f) OC emissions in July.

2.2. Aerosol model

The aerosol model is based on the scheme of Qian et al. (2001), which describes the SO_2/SO_4^{2-} system, completed by a parametrization of OC and BC compounds and assuming an external mixture of particles. The physico-chemical nature of carbonaceous aerosols is highly complex and variable, both at the emission and in the atmosphere, but in this first approach, we do not consider an explicit chemistry and physics of OC and BC. The OC aerosol field is assumed to encompass both primary direct emissions due to combustion processes and secondary OC particles formed from volatile hydrocarbon precursors. Because of its importance for removal processes and optical properties, the hygroscopicity of carbonaceous particles needs to be accounted for. We thus consider two states (hb = hydrophobic and hl = hydrophilic) for both OC and BC particles. Our model therefore includes six tracers: SO_2, SO_4^{2-}, OC_{hb}, OC_{hl}, BC_{hb} and BC_{hl}. For each tracer i, the corresponding mass-mixing ratio χ^i is calculated using the tracer transport equation

$$\frac{\partial \chi^i}{\partial t} = -\overline{V} \cdot \nabla \chi^i + F_H^i + F_V^i + T_C^i + S^i - R_{Wls}^i - R_{Wc}^i - D_d^i + \sum \left(Q_p^i - Q_l^i\right) \quad (1)$$

where the first four terms on the right-hand side of the equation represent advection, horizontal and vertical turbulent diffusion and convective transport, respectively (Qian et al., 2001). Following Kasibhatla et al. (1997), the convective-transport term assumes that the tracer becomes well mixed between cloud base and cloud top when cumulus convection occurs. S is the surface-emission term described in Section 2.3.

R_{Wls} and R_{Wc} in eq. (1) are the wet removal terms by large-scale and convective rain, (Giorgi, 1989; Giorgi and Chameides, 1986). The scavenging is function of the cloudwater to rainwater conversion rate, explicitly calculated for resolved clouds and specified for cumulus clouds, the grid cell cloud fraction (Pal et al., 2000) and the fraction of tracer dissolved into cloudwater: the later is assumed to be 0.95 and 0.05 for hydrophilic and hydrophobic OC and BC, respectively, 1 for SO_4^{2-} (Seinfeld and Pandis, 1998) and given by the cloudwater-dependent equilibrium dissolution value for SO_2 (Chameides, 1984). The scheme does not account for aerosol release by evaporation of raindrops.

Dry deposition D_{d} is treated in a simplified way by assuming fixed deposition velocities over land and water for each tracer. For SO_2, we specify deposition velocities of 0.8 cm s^{-1} over water and 0.3 cm s^{-1} over land (Tan et al., 2002). A deposition velocity of 0.2 cm s^{-1} is specified for SO_4^{2-} throughout the domain. Carbonaceous aerosol deposition velocities are taken from Cooke et al. (1999), i.e. 0.025 cm s^{-1} over land and 0.2 cm s^{-1} over water for hydrophilic aerosols and a constant velocity of 0.025 cm s^{-1} for hydrophobic aerosols.

In eq. (1), the terms Q_{p} and Q_{i} indicate production and losses due to physico-chemical transformations. For the sulphur compounds, the conversion of SO_2 to SO_4^{2-} occurs through both aqueous and gaseous pathways (Qian et al., 2001). The aqueous conversion implies the dissolution of SO_2 to form HSO_3^- and SO_3^{2-} ions and the further oxidation of these ions by O_3 and H_2O_2. As a first approximation, we here adopt the assumption of Giorgi et al. (2002), namely that the oxidation by H_2O_2 is dominant and never limited by the H_2O_2 concentration. This approximation relies upon the hypothesis of acidic conditions in cloudwater. In Europe, the cloudwater pH ranges typically between 4 and 6 (EMEP assessment report; http://www.emep.int), so that the assumption is realistic. The gaseous conversion is initiated by the oxidation of SO_2 by OH. In this study, the OH concentration field is fixed to an average value of 15×10^5 molecules cm^{-3} (Duncan et al., 2000) modulated by a superimposed diurnal cycle in which the OH concentration is close to zero at night. Qian et al. (2001) showed that the aqueous phase conversion pathway generally dominates and that the model is little sensitive to assumptions about the OH concentration.

Following Cooke et al. (1999), the ageing process of carbonaceous aerosol is simply represented by a transfer from the hydrophobic to the hydrophilic state with an exponential lifetime of $\tau_{ag} = 1.15$ d. The ageing of a particle is used to describe its coating by different chemical compounds (e.g. sulphate and volatile hydrocarbons) via gas to particle conversion processes (Riemer et al., 2004; Tsigaridis and Kanakidou, 2003; Cachier, 1998). Ageing thus depends on the chemical and meteorological environments, which are highly temporally and spatially variable at the regional scale. As described below, we test the model response to the value of τ_{ag} in a sensitivity experiment. Finally, aerosol concentrations are fixed to zero at the domain boundaries, assuming that external incoming aerosol amount is small compared to the sources.

2.3. Emission datasets

2.3.1. SOx emissions. The SO_2 and SO_4^{2-} (SO_x) primary emissions are calculated from the combination of two datasets. Over Europe, we use the EMEP (Cooperative Program for Monitoring and Evaluation of the Long-Range Transmission of Air Pollutant in Europe; http://www.emep.int/) emission database. This inventory provides annual emissions (Vestreng, 2003) of SO_x from 11 different activity sectors (power plant, traffic, agriculture, etc.) for the year 2000 at a 50-km resolution. For simplicity, we do not consider any temporal evolution of the SO_x emission. This strongly depends on the activity sectors and we assume that the seasonal cycle is small. Outside Europe, SO_x emissions are obtained from the public release of the EDGAR3.2 global database (Olivier et al., 2001). This inventory accounts for fossil- and biofuel combustions, industrial chemical production, biomass burning and waste treatment. The emissions of SO_x in this dataset are representative of the year 1995 and are originally provided at 1° resolution over the globe. In our baseline simulation, the EDGAR and EMEP sources have been combined and interpolated at the 60-km resolution RegCM domain (Fig. 1a). As outlined in Jeuken et al. (2001), the EMEP inventory shows substantially lower fluxes than the EDGAR database over Europe (Fig. 1b). A sensitivity experiment using both databases is presented in Section 4.

Two percent of the total sulphur emission is assumed to be in the form of SO_4^{2-} and the rest in the form of SO_2 (Qian et al., 2001). In addition, 70% of the sulphur is assumed to be emitted at the surface and thus occurs in the first model layer (∼45m) whereas the remaining 30% large-point emission is equally distributed between the second (110-m depth) and third (300-m depth) model layers above the surface (Qian et al., 2001). This data are in the range of the injection height given for the 11 EMEP emission sectors.

The largest sulphur emissions are found in central Europe, with large regional values and intense local sources corresponding to highly industrialized areas (Fig. 1a). Over the Mediterranean and middle-east regions, emissions are more sporadic and characterized by local intense sources, e.g. over the Arabic peninsula. Over West Africa, we note some relatively intense and extended sources primarily in the urbanized areas of Nigeria. Uncertainties in SO_2emissions are difficult to asses and depend strongly on the activity sector considered. In the EDGAR inventory, the uncertainty estimate varies from 10% for fossil fuel

Table 1. Number distribution characteristics and optical properties (at 380 and 550 nm) for the four carboneaceous types considered in the study. r_0 = 'dry' modal radius, σ = standard deviation, ρ_p = particle density, m = refractive index, σ_{ext} = dry extinction cross section, α hygroscopic growth parameter, $f_{rh=0.8}$ = hygroscopic growth factor at 80% relative humidity

Species	r_0 (μm)	σ	ρ_p (g cm^{-3})	$m = n\text{-}ik$ 380–550 nm	σ_{ext} (m^2 g^{-1}) 380 nm	550 nm	α	$f_{rh=0.8}$
BC_{hb}	0.0118	1.7	1.5	1.87–0.569i	14.6	9.6	0	0
BC_{hl}	0.03	1.9	1.5	1.87–0.569i	20.2	12.1	0.2	1.37
OC_{hb}	0.06	2.	1.7	1.55–0.005i	6.1	2.7	0	0
OC_{hl}	0.1	2.	1.7	1.55–0.005i	9.8	4.9.	0.25	1.49

combustion to 100% for industrial chemistry. The emissions are likely more accurate over Europe than the rest of the domain because they are generally better documented and make use of the updated and fine-scale EMEP inventory.

2.3.2. Carbonaceous emissions.

(i) The calculation of fossil fuel emissions of BC and OC aerosols is based on the method described in Cooke et al. (1999), which accounts for different types of fuel combustion and emission factors. In our study, the inventory is calculated for the year 1997 using updated algorithm compared to Cooke et al. (1999). Both primary OC and BC emissions are treated separately and provided globally at 1° resolution. On the basis of observations (Liousse et al., 1996) and detailed box model studies carried out in typical European urban environments, we multiply the primary OC emissions by a factor 1.25 to account for an implicit secondary OC production in anthropogenic plumes.

(ii) The biomass burning emission of OC and BC is described by Liousse et al. (1996). Savanna, forest, agricultural and domestic fire sources of carbonaceous particles are taken into account. The fluxes of organic matter and BC formed during the combustion process are calculated from detailed emission factors. The OC source is obtained for the total particle emission, and accounts for both primary and secondary organic particles. This inventory is typical of the decade (1980–1990) and is provided on a 5 × 3.75° global grid with a monthly resolution.

(iii) Both fossil fuel and biomass burning inventories are combined and interpolated onto the model grid to derive total OC and BC emissions (Figs. 1c–f). The highest emissions of BC are found over small regions of Europe in correspondence of high fossil fuel combustion areas (Figs. 1c and d). The biomass burning contribution is large in Africa, with extended sources characterized by a strong seasonality of BC and OC emissions. According to Liousse et al. (1996) the temporal distribution of forest and savanna fire (Figs. 1e and f) compares reasonably well with long term measurements and satellite observations during the 1980–1990 decade. However, for any given year, this pattern can be regionally modified by the rainfall amount and timing. The injection height of OC and BC follows the same approximation as in the sulphur emissions.

2.4. Aerosol optical depth

In Section 3.4 we validate the model results using the aerosol optical depth (AOD), which (for a given spectral interval) is calculated from the aerosol concentration and extinction coefficient (σ_{ext} m^2 g^{-1}) depending on the refractive index and the particle size distribution. The hygroscopic growth of hydrophilic aerosols and its influence on optical properties is taken into account. For sulphate, the parametrization of Kiehl et al. (2000) is used. For carbonaceous aerosol, the hygroscopic growth effect on the extinction coefficient is formulated as in Kasten (1969): $\sigma_{ex} = \sigma^d_{ex} \cdot (1 - RH)^{-\alpha}$ where σ^d_{ex} is the extinction coefficient for low relative humidity and α is an empirical parameter ranging from 0 to almost 1 for highly soluble species. The values proposed in Table 1 are mainly based on biomass burning smoke studies (Reid et al., 1998, 2005). The hygroscopic growth function at 80% is also reported in Table 1. We assume that the aged BC core is surrounded by a hydrophilic shell for which water affinity is lower than for aged OC, which is itself less hydrophilic than sulphate.

Dry values of the extinction coefficient are calculated using a Mie code (Mätzler, 2002) assuming refractive indices and log-normal size distributions (Table 1). The refractive indices of carbonaceous particle are very variable, with subsequent uncertainties on the optical parameters (Reid et al., 2005). Mean geometric radii describing the dry particle distribution are assigned as a function of the different types of aerosols. Hydrophobic components, corresponding to young aerosols, are characterized by a radius smaller then for the aged components (Mallet et al., 2003; Reid et al., 1998). The corresponding specific extinction cross sections are also reported in Table 1. According hb/hl emission ratio, a rough estimate of the dry carbonaceous aerosol extinction cross section is 3.8 m^2 g^{-1} near the sources and increasing to 5 m^2 g^{-1} as the smoke ages. These values are in the range given by literature (Penner et al., 2001).

Previous studies (Liousse et al., 1997; Seinfeld and Pandis, 1998) show that the extinction cross section is weakly sensitive to the mixing hypothesis because the perturbations on absorption and scattering cross sections tend to compensate. For the purpose of aerosol field validation at the regional scale (Section 3.3),

the assumption of external mixing to calculate the optical depth seems then reasonable. It is however important to emphasize that the mixing state affects the single scattering albedo and should be considered for further aerosol radiative forcing and climatic impact studies.

3. Model comparison against observations

3.1. Brief description of the climatology of the simulated periods

The simulated average precipitation rates for DJF and JJA are compared to observe precipitation provided by the Climatic Research Unit (CRU) of the University of East Anglia in Fig. 2. The corresponding simulated average low-level wind fields are also shown in Figs. 2b and d.

In DJF (Figs. 2a and b), the north European sector of the domain is dominated by a relatively intense westerly circulation, with maximum precipitation occurring throughout western, central and southern Europe. The model reproduces well the observed precipitation patterns, with a slight underestimation over the UK and an overestimation in areas of central and eastern Europe. Regional topographically induced precipitation patterns (e.g. over the Alps and Balkans) are correctly simulated by the model. The mean simulated precipitation patterns over the Mediterranean basin are in agreement with observations and the dominant average low-level circulation is northwesterly over the central Mediterranean. Over Africa, the sub equatorial rainfall patterns are also satisfactorily simulated by the model in DJF, with possibly local overestimates over the mountainous regions of Gabon and Congo (although the observed data may highly be uncertain there). In particular, the northern geographical limit of rainfall is well represented (Fig. 2b). The Harmattan northeasterly flux over the Sahara and Sahelian region is clearly represented in the simulation.

In JJA (Figs. 2c and d), the simulated westerly circulation is much weaker than in winter and the position of Azores anticyclone is clearly represented. Extensive precipitation occurs

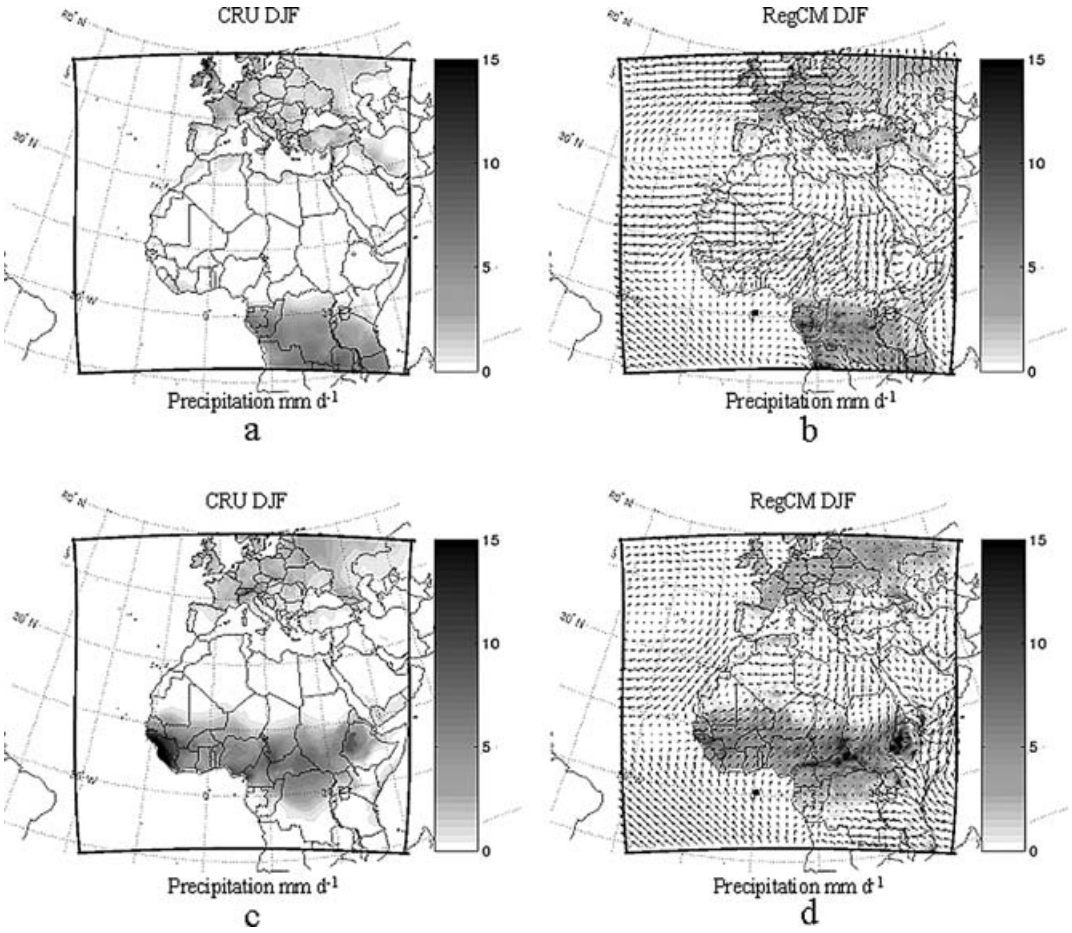

Fig 2. Comparison between observed and simulated precipitation rates (mm d^{-1}) for DJF and JJA 2000. (a) CRU observations, DJF 1999–2000; (b) Average RegCM precipitation and low-level wind (sigma = 0.970), DJF 1999–2000; (c) CRU observations, JJA 2000; (d) Averaged RegCM precipitations and low-level wind (sigma = 0.970), JJA 2000.

throughout central and eastern Europe with a reasonably good agreement with observations. Precipitation tends to be more convective in summer than in winter, which affects the vertical transport of tracers. The Mediterranean regions experience their dry season in summer and this is well simulated by the model except for an overestimation over northern Algeria and the Atlas region. Low-level winds over southern Europe and the eastern Mediterranean basin are predominantly from the north. The African monsoon circulation and rainfall patterns over sub-Saharan Africa are captured by the model. We note however an underestimation of the observed rain maximum over the coastal regions of Guinea and an overestimation over the mountainous regions of Central Africa and Ethiopia. Again, the observations may be characterized by relatively large uncertainties over these data-sparse regions. The northward extent of the monsoon precipitation belt is in general agreement with observations, showing only a slight northward shift over West Africa. The southward extent of the precipitation belt over Congo is well simulated. Concerning the winds, easterly and southerly low-level flow dominates especially over eastern Africa.

Overall, the results shown in this section indicate that the model captures the basic circulation and rain patterns over the simulation domain for both the summer and winter cases.

3.2. Evaluation of near-surface concentrations

The number and quality of observations we were able to find are very variable across our simulation domain. For sulphur compounds, the analysis focuses mainly on the European sector of the domain and it is based on the EMEP measurement network (http://www.nilu.no/projects/ccc/) for the winter and summer of 2000. This comparison is strengthened by the fact that we used specific sulphur emissions representative of the year 2000 over the European region. For carbonaceous aerosols, we used data collected over the past 15 yr either during specific observation campaigns (Tables 2b and 3b) or from EMEP particulate matter (PM) analysis in the year 2000. This approach is also consistent with the fact that the carbonaceous emission inventories are not specifically representative of 2000.

3.2.1. SO_2/SO_4^{2-}. Because we are interested in the climate application of our model, we evaluate here the ability of the model to reproduce the average seasonal spatial distribution of sulphate, rather than given pollution episodes (which would require much more details in source and chemical parametrization). Therefore, monthly averaged SO_2 and SO_4^{2-} simulated concentrations at the model bottom layer are compared with monthly averaged measurements given over the EMEP European station network (for D 1999 JF 2000 and JJA 2000). The seasonally averaged comparisons are synthesized in Figs. 3 and 4 for DJF and JJA. Monthly spatial correlation coefficients (COR) and root mean square (RMS) errors between monthly simulation results and EMEP monthly data have been also calculated (the number of observing stations being between 84 and 91 for SO_2 and between 74 and 79 for sulphate). The seasonal spatial RMS and COR have been obtained by averaging the monthly RMS and COR for DJF and JJA.

The simulated sulphate distribution (Figs. 3c and d) shows maximum concentrations over central Europe in proximity of the high-emission sources of SO_2. The sulphate field tends to be more spread out than the SO_2 field, indicating a fast SO_2 to SO_4^{2-} conversion. Sulphates are also more effectively spread out in winter due to the stronger eastward advection by the prevailing westerly winds (Figs. 2 and 3).

For sulphates, in DJF, a COR of 0.60 is obtained between model values and measurements, with an associated RMS error 0.37 μg m^{-3} and 57% of the modelled value ranging in the a factor of 2 compared to observations. The model performance tends to degrade in JJA with a COR of 0.40 and a RMS of 0.61 μg m^{-3} and 34% of the value ranging in a factor of 2. The COR are statistically significant at the 99% confidence level in both DJF and JJA. In addition, these results are comparable to those found in the model inter-comparison of van Loon et al. (2004), who found values of COR obtained using different CTMs over the European region (compared to EMEP data) in the range of 0.35–0.45 for SO_2 and 0.37–0.67 for sulphate. However, the scatter plots (Figs. 4c and d) reveal a general underestimation of the simulated sulphate concentration over Europe. This underestimation is notably more pronounced in summer than in winter. An analysis of the SO_2 sulphate precursor (Figs. 4a and b) shows a slight underestimation in DJF and overestimation in JJA, with these tendencies being much less evident than for sulphates.

Regionally, the sulphate-simulated field tends to match better the observations in northern and central Europe than in the Mediterranean region (Figs. 3c and d). In particular, the concentration patterns and gradients over central Europe (high-emission area) are well captured. Some local high sulphate concentration areas (e.g. northern Italy) are nevertheless underestimated. The underestimation bias in Mediterranean region (mainly over Spain where most of the available observations are located) appears also to be much larger in summer than in winter.

A number of factors can contribute to explain the discrepancies between simulated and observed EMEP concentrations.

(i) The model does not capture some local features. Intense local SO_2 emissions are smoothed by the grid averaging, e.g. over the northwestern coasts of Spain or the area around Rome and Milan. Note that seashore stations can be affected by sulphates contained in marine aerosol and not accounted for in this study. On the other hand, surface concentrations may be overestimated over mountainous stations (e.g. Switzerland), where the model 60-km resolution does not capture accurately the topography.

(ii) For a number of stations, the sulphate concentrations are underestimated, while the SO_2 precursor is well simulated (e.g. Spain in Fig. 3, and the scatter plots of Fig. 4). This suggests some model limitations concerning transport and removal processes of the sulphate. Particularly, the wet deposition of sulphate might

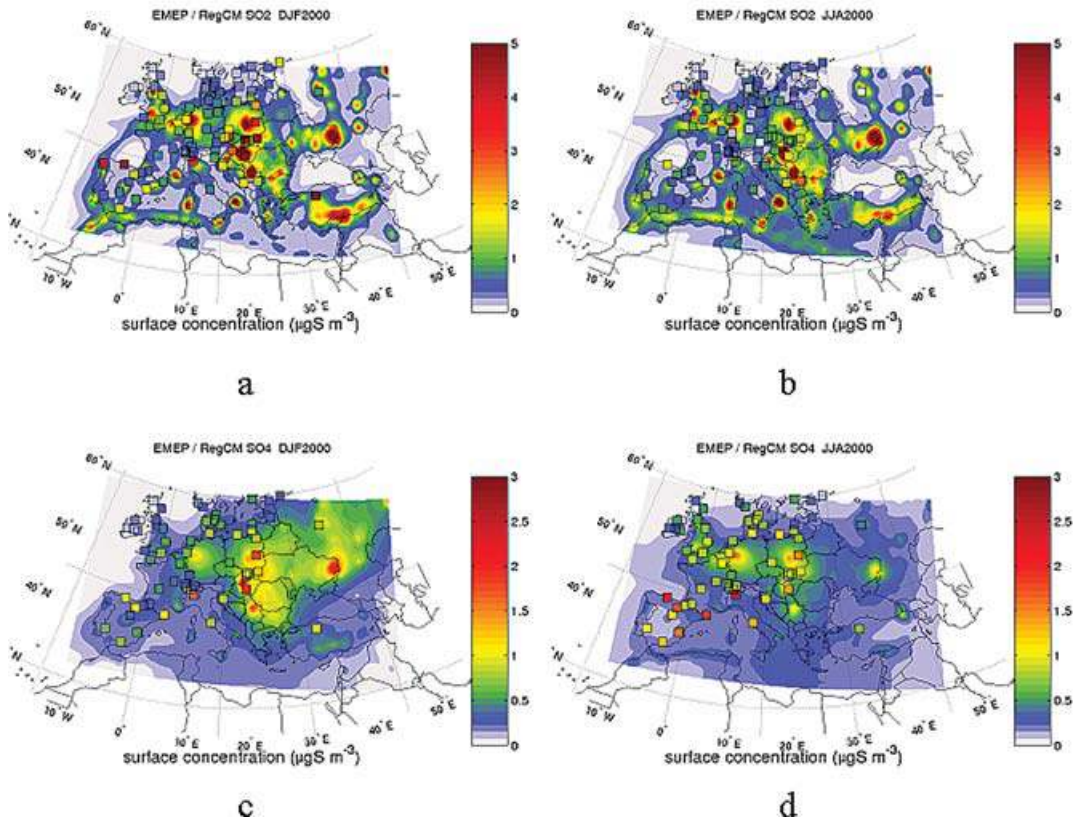

Fig 3. Comparison between simulated sulphur compound surface concentrations (μg S m^{-3}) and measurements over the EMEP network (represented by coloured squares). (a) SO_2 averaged for DJF; (b) SO_2 averaged for JJA; (c) SO_4^{2-} averaged for DJF; (d) SO_4^{2-} averaged for JJA.

be overestimated, as the release of sulphate by re-evaporation of cloud droplet is not accounted for in the model. Sulphate is also affected by the representation of transport by convective processes: the underestimation of surface concentrations, especially in summer, may be an indication of excessive vertical convective transport in the model.

(iii) The assumptions made in the simple SO_x chemical scheme can lower the sulphate production rate. Particularly, in summer and for dry conditions (Mediterranean area), the photochemical production of OH is likely to be underestimated: monthly OH concentration can be substantially greater than the assumed averaged OH concentration. This leads to an underestimation of SO_2/SO_4^{2-} conversion by the gaseous pathway. Moreover, the aqueous sulphate production via the O_3 oxidant has been neglected, and this can lead to an underestimation of sulphates especially in regions of pH $>$ 5 and high levels of ozone. Once again, such conditions are likely to occur in the Mediterranean region, which is influenced by alkaline mineral dust and where an active ozone photochemistry takes place.

These different processes are often cited as the main cause of variability when comparing different sulphate models (Roelofs et al., 2001; Reid et al., 2005). In particular, the tendency of models to be less successful in simulating sulphate over the Mediterranean than central and northern Europe has been emphasized in detailed chemistry studies involving the unified EMEP model (e.g. EMEP report 2003).

Over equatorial Africa, biomass burning generates low level of sulphate aerosol and in fact most of the sulphur emission derives from anthropogenic fossil fuel combustion. Measurements of sulphur compounds over equatorial Africa are still scarce. Ongoing experiments carried out in extended urban areas of West Africa (February and March 2004) found SO_2 concentrations reaching 6 ppb for Dakar (Yoboué, personal communication) and 2 ppb for Abidjan (Ndiaye, personal communication). By comparison, the model simulates SO_2 concentrations of the order of 0.3 ppb over Abidjan and Dakar. The maximum concentrations are obtained for the Lagos region with $\sim$3 ppb. These discrepancies can be at least partially explained by the grid averaging effect. However, the EDGAR sulphur sources of these urban regions are very uncertain and likely to be underestimated.

3.2.2. Carbonaceous aerosols. Regarding experimental data, attention must be paid to the analytical method ('optical' or 'thermal') used to measure OC and BC concentrations. Intercomparison studies show that even if the total carbonaceous particle retrievals are in agreement between the two methods, large discrepancies can still be found in the separation of the OC and

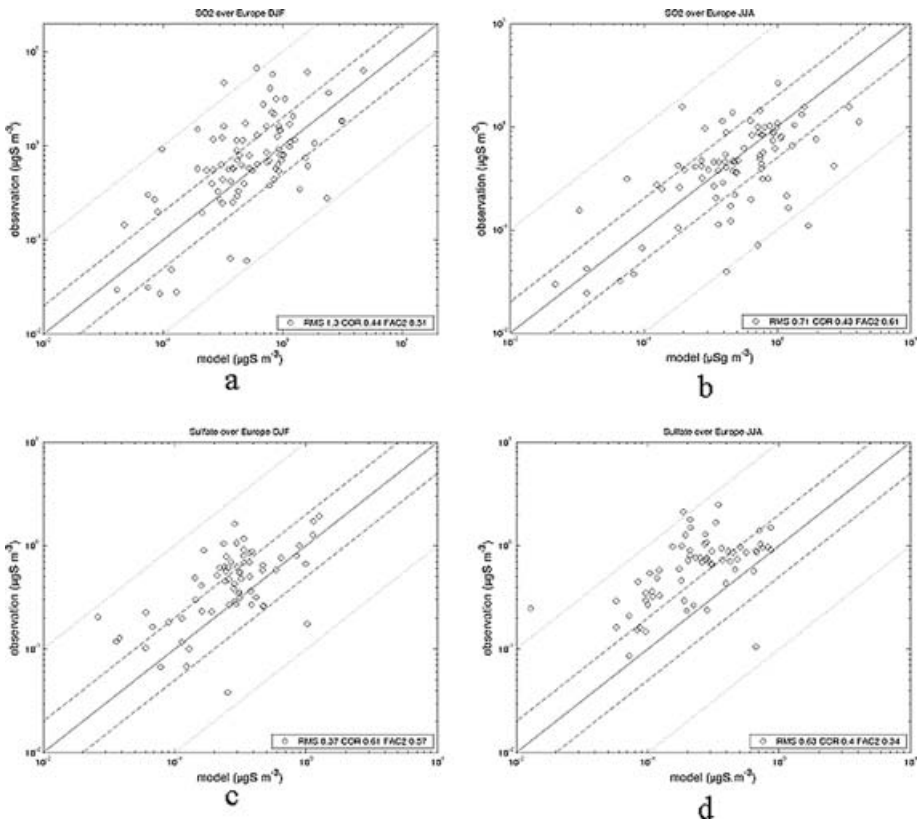

Fig 4. Scatter plot of simulated versus observed values of surface concentration for sulphur compounds over Europe (see also Fig. 3): (a) SO_2, DJF; (b) SO_2, JJA; (c) SO_4^{2-}, DJF; (d) SO_4^{2-}, JJA. Seasonal statistics are calculated from monthly data (see text) collected over a number of stations ranging between 84 and 91 for SO_2 and 76 and 79 for sulphates: COR is the spatial correlation coefficient. RMS the root mean square error (in μg m^{-3}) and FAC2 the fraction of simulated values ranging in a factor of 2 compared to observations.

BC components (up to 46% standard deviation, Schmid et al., 2001). Keeping this in mind, different datasets are used here for the validation of OC and BC surface concentrations.

(i) Tables 2a and 3a present observed values of OC and BC concentrations derived from Putaud et al. (2003). These values were measured over some EMEP stations during the last 10 yr. The analytical methods used for these measurements were not specified. Stations corresponding to kerbside, representative of local sources, have been rejected. (ii) Tables 2b and 3b also report measured data issued from specific field campaigns and referred in the literature. Data issued from optical measurement methods have been specified here.

(ii) Finally, we also estimated OC and BC concentrations using PM measurement collected over the EMEP network during the winter and summer of 2000. For these latter values, the estimation of BC content was carried out assuming that BC accounts for 8% of the $PM_{2.5}$ and 5% of the PM_{10} mass. For OC, we assumed that organic matter (OM) accounts for 22% and 25% of $PM_{2.5}$ and PM_{10}, respectively. These ratios have been estimated using an average composition as determined by Putaud et al. (2003) over the EMEP network, and are in agreement with data usually observed. In addition, we assume a ratio of ($OM/OC = 1.3$) to estimate the amount of OC (Liousse et al., 1996).

From these three different datasets, the corresponding simulation versus observation scatter plots are shown in Fig. 5.

3.2.2.1. Black carbon. Figure 5a illustrates the model performance against the datasets in DJF and JJA. About 56% in DJF and 62% in JJA of the simulated values are within a factor of 2 of the corresponding measured values. Following the IPCC model inter-comparison shown in (Penner et al., 2001, Fig. 5.10) and in view of the uncertainties in the methods of observations of BC (see above), the model BC predictive capability appears to be in line with that of state-of-the-art CTMs. However, an overall substantial uncertainty is still evident from the data in Fig. 5. We also note that a model underestimate is evident for the urban stations (Tables 2a and b), suggesting a problem of point source representation at the 60-km model grid. High underestimations are also found specifically over Portugal, possibly due to the lack of temperate vegetation fires (occurring mostly in Mediterranean regions in summer) in the biomass burning inventory (which just account for 'clearing' activities over Europe). In contrast, the error for the measurements collected in 2000 is smaller than

Table 2. (a) Observed and simulated BC surface concentration in Europe for DJF and JJA. Data are from a statistical analysis of Putaud et al. (2003). (b) Observed and simulated BC surface concentration based on a number of studies reported in the literature. (O) stands for optical methods (see text). UM stands for 'unpublished manuscript'

(a)

				BC (μg m^{-3})			
lat	Lon	Site		Obs DJF	Mod DJF	Obs JJA	Mod JJA
58.82	6.72	Natural	Skreadalen (N)	0.57	0.15	0.35	0.14
58.38	8.25	Natural	Birkenes (N)	0.55	0.23	0.37	0.15
35.32	25.67	Natural	Finokalia (GR)	0.66	0.34	2.27	0.59
47.05	7.58	Rural	Chaumont (CH)	0.37	1.00	0.50	0.90
40.50	−0.20	Rural	Monagrega (E)	0.43	0.46	0.40	0.30
48.23	16.36	Rural	Illmitz (A)	2.74	1.71	0.66	1.53
51.12	41.08	Near-city	Waasmunster (B)	1.29	1.72	1.12	0.67
51.53	12.93	Near-city	Melpitz 96-99 (D)	1.54	2.54	1.12	2.17
45.82	8.63	Near-city	Ispra (I)	2.05	1.29	1.65	0.99
43.35	5.40	Urban	Marseille-VD (F)			1.14	0.85
47.37	8.53	Urban	Zuerich (CH)	2.42	1.77	1.31	1.52
47.53	7.58	Urban	Basel (CH)	2.12	1.13	1.17	1.04
51.02	3.73	Urban	Gent (B)	1.93	1.18	1.46	1.54
44.53	11.29	Urban	Bologna (I)	4.08	1.09	1.58	0.81
45.53	9.20	Urban	Milano-Bresso (I)			2.55	1.46

(b)

				BC (μg m^{-3})				
Lat	lon	Site		Obs DJF	Mod DJF	Obs JJA	Mod JJA	Ref
53.30	−9.90	Marine	Mace Head	0.066	0.037	0.126	0.10	Junker 2000 (Pers. Comm.) (O)
52.90	3.00	Rural	Petten (N)	1.63	0.30			Berner et al. (1996) (O)
52.40	1.40	Rural	Hemsby (GB)	0.10	0.64	0.10	0.64	Yaaqub et al. (1991) (O)
52.00	5.70	Rural	Wageneinen (N)	18.00	1.30			Janssen et al. (1997) (O)
51.00	−1.00	Rural	Edgbaston (GB)	0.60	0.79	0.60	1.03	Smith et al. (1996)
51.00	12.00	Rural	Melpitz (D)	2.30	1.88	2.30	1.75	Heintzenberg et al. (1998)
48.80	2.33	Urban	Paris(F)	2.35	1.40	2.35	1.63	Cachier et al. (2004)
48.26	15.93	Urban	Vienna (A)	4.4	1.40	2.7	1.31	Salam et al., UM
48.21	16.33	Rural	Streithofen (A)	2.2	1.39	1.6	1.30	Salam et al., U.M
47.00	13.00	Remote	Sonnblic (A)			5.00	0.70	Hitzenberger et al. (1999) (O)
46.90	19.50	Rural	KPuszta (HR)	0.81	1.79	0.50	1.48	Molnar et al. (1999)
46.30	14.50	Remote	Krvavec (SL)	0.15	0.74	0.45	0.55	Bizjak et al. (1999) (O)
45.48	9.19	Urban	Milan (I)	2.66	1.18	2.66	0.95	Cachier et al. (2004)
44.70	11.60	Rural	SanPietro (I)			1.00	0.70	Zappoli et al. (1999)
43.78	11.24	Urban	Florence (I)	2.4	0.75	2.4	0.65	Cachier et al. (2004)
43.40	5.05	Indust	Martigues (F)			2.32	0.71	Cousin et al., UM
43.30	5.38	Urban	Marseille (F)			2.6	0.72	Cousin et al., UM
42.93	0.15	Remote	Pic du midi (F)	0.025	0.31	0.15	0.27	Galy-Lacaux et al. (2004)
42.00	9.00	Marine	Corsica (F)	0.38	0.36			Cachier et al. (1989)
41.50	42.70	Rural	Mt kanobily (GE)			1.09	0.28	Dzubay et al. (1984)
41.00	5.00	Marine	West-Med	0.40	0.30	0.40	0.25	Cachier et al. (1990)
40.50	−8.80	Marine	Areao (P)	0.37	0.34	0.59	0.28	Pio et al. (1996)
40.30	−8.40	Rural	Anadia (P)			1.59	0.30	Castro et al. (1999)
40.00	−8.00	Rural	Aveiro (P)			11.80	0.30	Nunes and Pio (1996)
33.00	−17.00	Rural	Tabua (P)			1.17	0.04	Castro et al. (1999)
6.20	−5.10	Rural	Ivory Coast	1.30	1.59	0.20	0.09	Wolff and Cachier (1998), Cachier et al. (1989, 1990)
2^{-}12	17–19	Rural	Central Africa	3.36	1.67			Ruellan et al. (1999)

Table 3. Same as Table 1 but for OC particles

(a)

				OC (μg m^{-3})			
Lat	lon	site		Obs DJF	Mod DJF	Obs JJA	Mod JJA
58.82	6.72	Natural	Skreadalen (N)	0.67	0.19	0.75	0.12
58.38	8.25	Natural	Birkenes (N)	0.54	0.32	0.83	0.13
35.32	25.67	Natural	Finokalia (GR)	1.35	0.75	3.24	1.24
47.05	7.58	Rural	Chaumont (CH)	0.99	1.29	1.60	0.78
40.5	−0.2	Rural	Monagrega (E)	1.24	0.66	1.14	0.29
48.23	16.36	Rural	Illmitz (A)	1.24	3.03	1.31	2.60
51.12	41.08	Near-city	Waasmunster (B)	2.76	3.66	3.73	1.08
51.53	12.93	Near-city	Melpitz 96-99 (D)	3.14	4.29	1.60	3.49
45.82	8.63	Near-city	Ispra (I)	4.18	1.51	2.36	0.82
43.35	5.4	Urban	Marseille-VD (F)		0.99	2.85	0.63
47.37	8.53	Urban	Zuerich (CH)	4.63	2.32	2.61	1.67
47.53	7.58	Urban	Basel (CH)	4.72	1.58	2.03	1.07
51.02	3.73	Urban	Gent (B)	0.99	1.18	3.36	1.35
44.53	11.29	Urban	Bologna (I)	9.48	1.37	3.01	0.76
45.53	9.2	Urban	Milano-Bresso (I)			9.45	0.91

(b)

				BC (μg m^{-3})				
Lat	lon	Site		Obs DJF	Mod DJF	Obs JJA	Mod JJA	Ref
48.80	2.33	Urban	Paris(F)	6.07	1.31	6.07	1.22	Cachier et al. (2004)
45.48	9.19	Urban	Milan (I)	6.62	1.40	6.62	0.78	Cachier et al. (2004)
44.70	11.60	Rural	SanPietro (I)			6.20	0.68	Zappoli et al. (1999)
43.78	11.24	Urban	Florence (I)	8.37	0.96	8.37	0.60	Cachier et al. (2004)
43.40	5.05	Dust	Martigues (F)			3.00	0.10	Cousin et al. UM
43.30	5.38	Urban	Marseille (F)			5.38	0.53	Cousin et al. UM
42.93	0.15	Remote	Pic du midi (F)	0.07	0.6	0.69	0.22	Galy-Lacaux et al. (2004)
42.00	9.00	Marine	Corsica (F)	1.52	0.58			Cachier et al. (1989)
41.50	42.70	Rural	Mt kanobily (GE)			2.46	0.55	Dzubay et al. (1984)
41.00	5.00	Marine	West-Med	1.60	0.45	1.60	0.23	Cachier et al. (1990)
40.50	−8.80	Marine	Areao (P)	0.94	0.36	1.41	0.21	Castro et al. (1999)
40.30	−8.40	Rural	Anadia (P)			3.51	0.25	Castro et al. (1999)
40.00	−8.00	Rural	Aveiro (P)	7.40	0.46	7.40	0.25	Nunes and Pio (1993)
33.00	−17.00	Rural	Tabua (P)			5.83	0.04	Castro et al. (1999)
7.00	18.00	Rural	Central Africa	13.02	10.18			Ruellan et al. (1999)
6.20	−5.10	Rural	Ivory Coast	9.20	10.03	1.20	0.44	Wolff and Cachier (1998), Cachier et al. (1989, 1990)

that of the other data (Figs. 5a and c), most likely because the meteorological context is more specifically represented by the model for this dataset. Finally, the larger biases are found when comparing model results with measurements obtained by the optical method.

Unfortunately, only a few direct measurements of BC are available over the African portion of the domain. We report in Table 2a values collected in central Africa from November to December (Ruellan et al., 1999) and for a savanna ecosystem in Ivory Coast in fall and winter (Cachier et al., 1990). Simulated values agree with the observed ones within a factor of about 2 and are consistent with other studies (e.g. Chung and Seinfeld, 2002). In particular, the model captures the strong seasonality of the BC induced by biomass burning over the Ivory Coast (see also Liousse et al., 1996).

3.2.2.2. Organic carbon. About 64% of the modelled OC values are within a factor of 2 of the observations for DJF, these value decreasing to 33% in JJA. Figure 5b and d shows a general underestimation in the simulated values, particularly in summer. This underestimation bias may be due to a number of reasons.

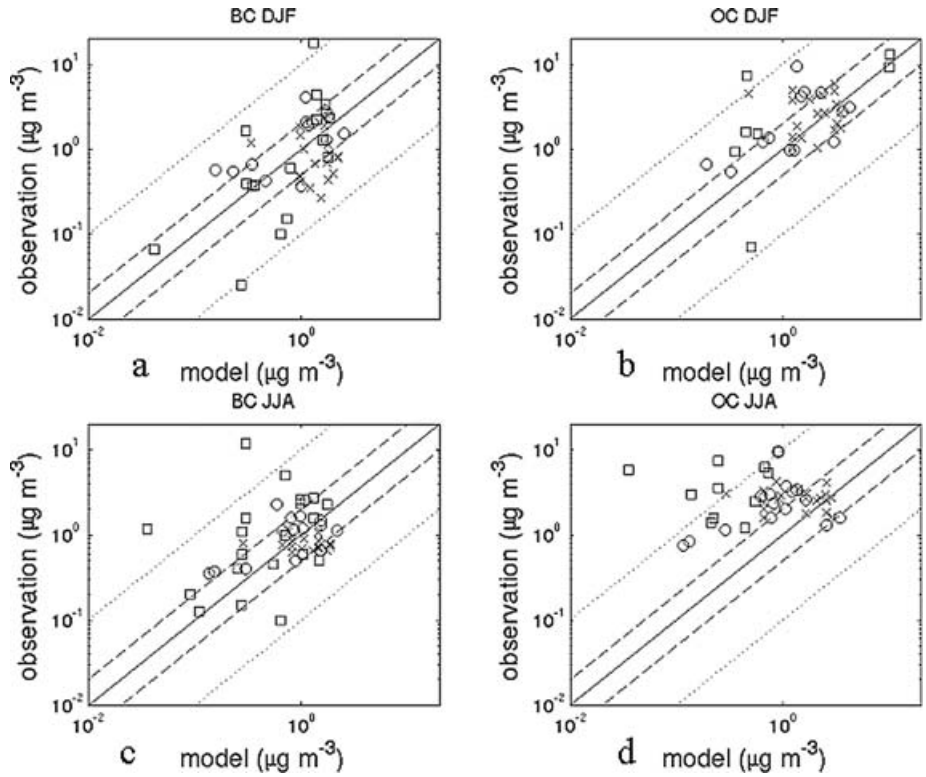

Fig 5. Scatter plot of simulated versus observed values of surface concentrations of carbonaceous compounds. (○) BC, OC concentration in Europe (from Putaud et al., 2003; see also Tables 2a and 3a), (□) Bibliographical data (see references in Tables 2b and 3b), (×) Estimation of BC and OC concentrations based on EMEP particulate matter measurements over Europe (specific year 2000) and Putaud et al. (2003) carbonaceous matter fractions (see text). (a) BC, DJF; (b) OC, DJF; (c) BC, JJA; (d) OC, JJA.

(i) Uncertainties in OC sources (Cooke et al., 1999; Liousse et al., 1996; Penner et al., 2001) are still very high. Among different factors, the proportion of OC/OM considered for fossil fuel emissions may be highly variable according to the actual aerosol age and the underlying type of combustion. Moreover, as for BC, some sources (e.g. the temperate vegetation fires, vegetative debris) are not accounted for in the present inventory. (ii) The assumption of a constant factor to derive secondary OC from the primary emissions. Secondary OC formation is complex and variable, depending on the chemical and meteorological context and the nature of precursor sources (Chung and Seinfeld, 2002). In particular, secondary OC aerosols issued from biogenic precursors are not accounted for in this work. This could partly explain the higher biases in summer and over Mediterranean regions (e.g. Portugal in Table 3). (iii) As for sulphate and BC, uncertainties in vertical convective transport and removal processes (notably OC hygroscopicity) also directly affect the simulated surface concentrations.

For African locations (Table 3b), the concentrations of OC are particularly high and seasonal due to the biomass burning sources. The simulated concentrations are in agreement with the few available measurements and with other studies (Chung and Seinfeld, 2002).

3.3. Comparison with AOD data

As an additional validation tool, we compare simulated and observed AOD. This comparison is necessarily limited by the fact that our model does not account for all aerosols (as the observed AOD does), however, it can still provide valuable information especially in regions dominated by anthropogenic aerosols and where direct measurements are rare (e.g. the biomass burning regions of Africa). In addition, while the validation presented in the previous sections was limited to the surface concentrations, the AOD provides information on the aerosol column burden.

Figure 6 shows simulated AOD (550 nm), as calculated in Section 2.3 for each model aerosol type. Figures 7a and b and 8a and b present the simulated total anthropogenic optical thickness at 550 nm and 380 nm. For both wavelengths, we compare the model AOD fields to point values issued from the AERONET sun photometer federal network (Holben et al., 1998), retaining stations showing enough continuity (Figs. 7a, b, 8a and b). To analyse regional patterns, we also use satellite AOD: for the 550-nm wavelength, we use the MODIS (Tanré et al., 1999; Kaufman et al., 1997) AOD fine fraction product (more representative of anthropogenic compounds, smoke and dust fine mode) and the MISR AOD (Martonchik et al., 1998). These products

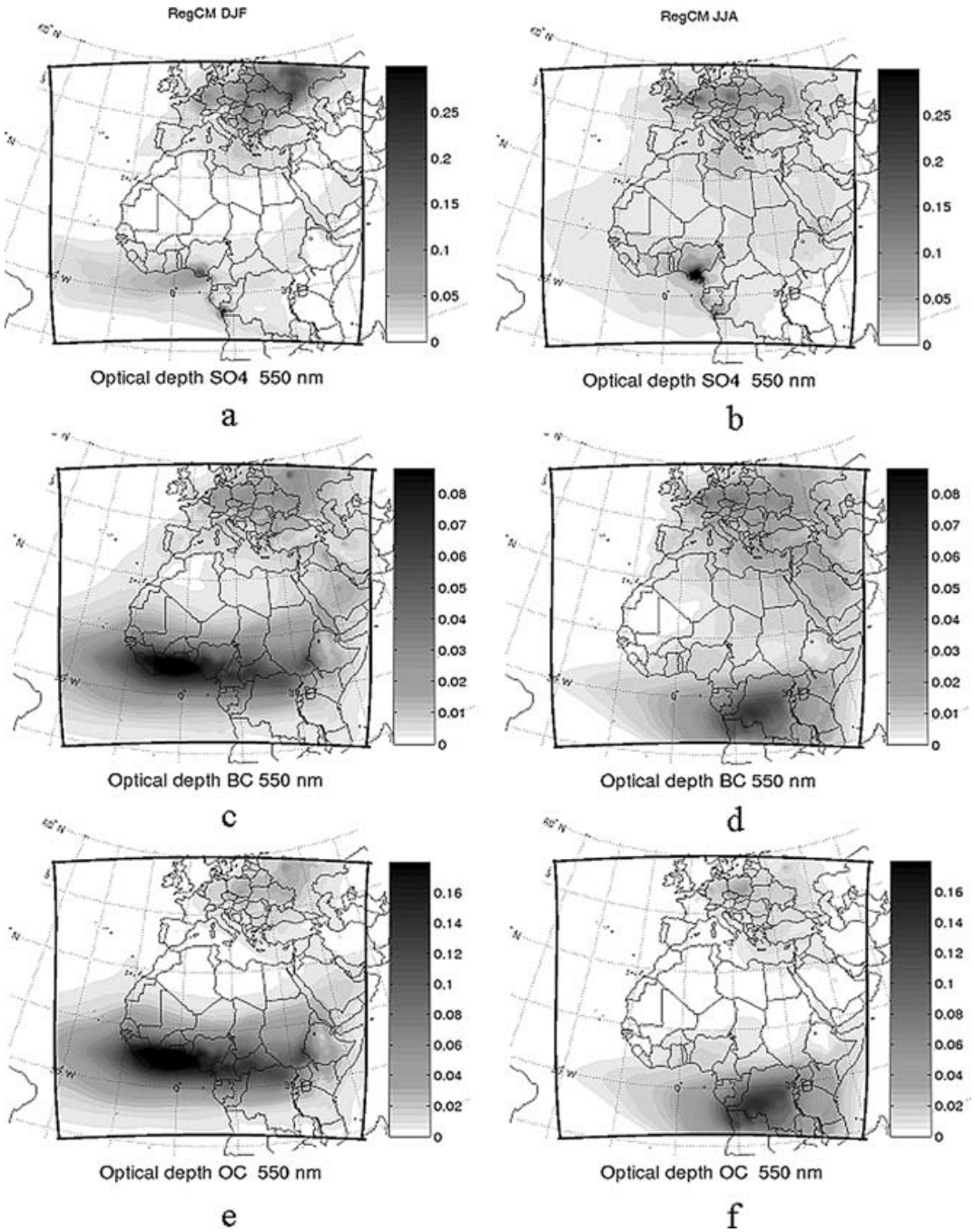

Fig 6. Simulated AOD at 550 nm for different types of anthropogenic particles. (a) SO_4^{2-}, DJF; (b) SO_4^{2-}, JJA; (c) BC, DJF; (d) BC, JJA; (e) OC, DJF; (f) OC, JJA.

are limited to JJA 2000 (Figs. 7c and d). In the UV (380 nm), we use the TOMS AOD retrieval (Torres et al., 1998), which is mainly sensitive to absorbing smoke and dust. This product is available for both DJF and JJA (Figs. 8c and d). Comparative evaluations of these different datasets are available in the literature (Ichoku et al., 2004; Myhre et al., 2004; Torres et al., 2002).

3.3.1. Europe. The simulated AOD over the European region is dominated by the sulphate contribution, which can reach seasonally averaged values of 0.3. The contributions of BC and OC are roughly five and three times lower in magnitude, respectively (Fig. 6).

Comparison with available AERONET AOD reveals a quite good agreement (within a factor of 1.5) between simulated and

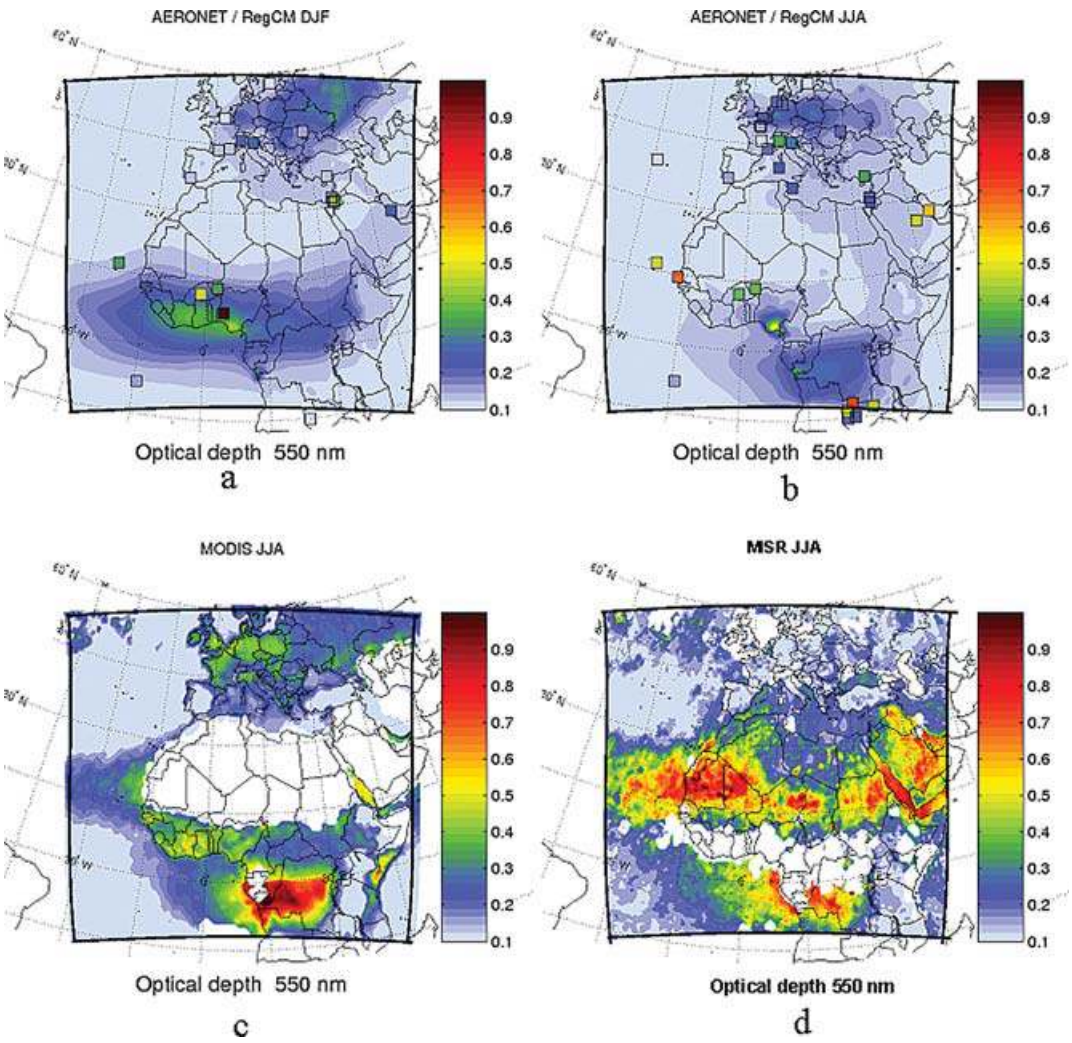

Fig 7. (a) Simulated AOD at 550 nm compared with averaged AERONET AOD measurements (coloured squares) for DJF. (b) Same as (a) but for JJA. (c) MODIS AOD retrieval (small particle fraction at 550 nm) for JJA 2000 (the white areas indicate no data availability). (d) MISR AOD retrieval (550 nm) for JJA 2000 (the white areas indicate no data availability).

observed AOD over northern Europe (e.g. Germany) in the visible and UV range, and for both seasons (Figs. 7a, b, 8a and b). As pointed out for the surface concentrations, the AOD over some highly urbanized areas is underestimated compared to AERONET DATA (e.g. northern Italy). Considering regional AOD patterns for JJA, the MODIS AOD (Fig. 7c) is about two times larger than both the simulated and AERONET AOD, especially over land. This points to a significant uncertainty in the observations themselves. The position of AOD maxima is nevertheless consistent between RegCM and MODIS results. The MISR AOD (Fig. 7d) is much lower and closer to the model results in magnitude, but shows a rather noisy spatial distribution and the related patterns are difficult to interpret. Some studies suggest a positive bias in the MODIS AOD (Stier et al., 2005) over land. Nevertheless, a tendency of the model to underestimate European AOD is expected as nitrates (see notably Schaap et al., 2003), marine aerosols and biogenic SOA are not accounted for.

3.3.2. Mediterranean Basin. Over the Mediterranean basin, the simulated AOD systematically underestimates the AERONET data (Figs. 7a, b, 8a and b). This bias is larger in summer, as also confirmed by the regional MISR JJA retrievals (Fig. 7d). The underestimation is primarily linked to North African desert dust, as particularly visible over western Mediterranean (see TOMS data in Fig. 8c) and Arabic Peninsula in JJA (see TOMS and MISR data). The underestimation over Cairo likely results from the lack of dust particle but also from a possible underestimation of the local anthropogenic emissions.

Contribution of the dust is theoretically minimized in the MODIS small fraction product (Fig. 7c). The simulated and MODIS AOD are closer to each other over the Mediterranean

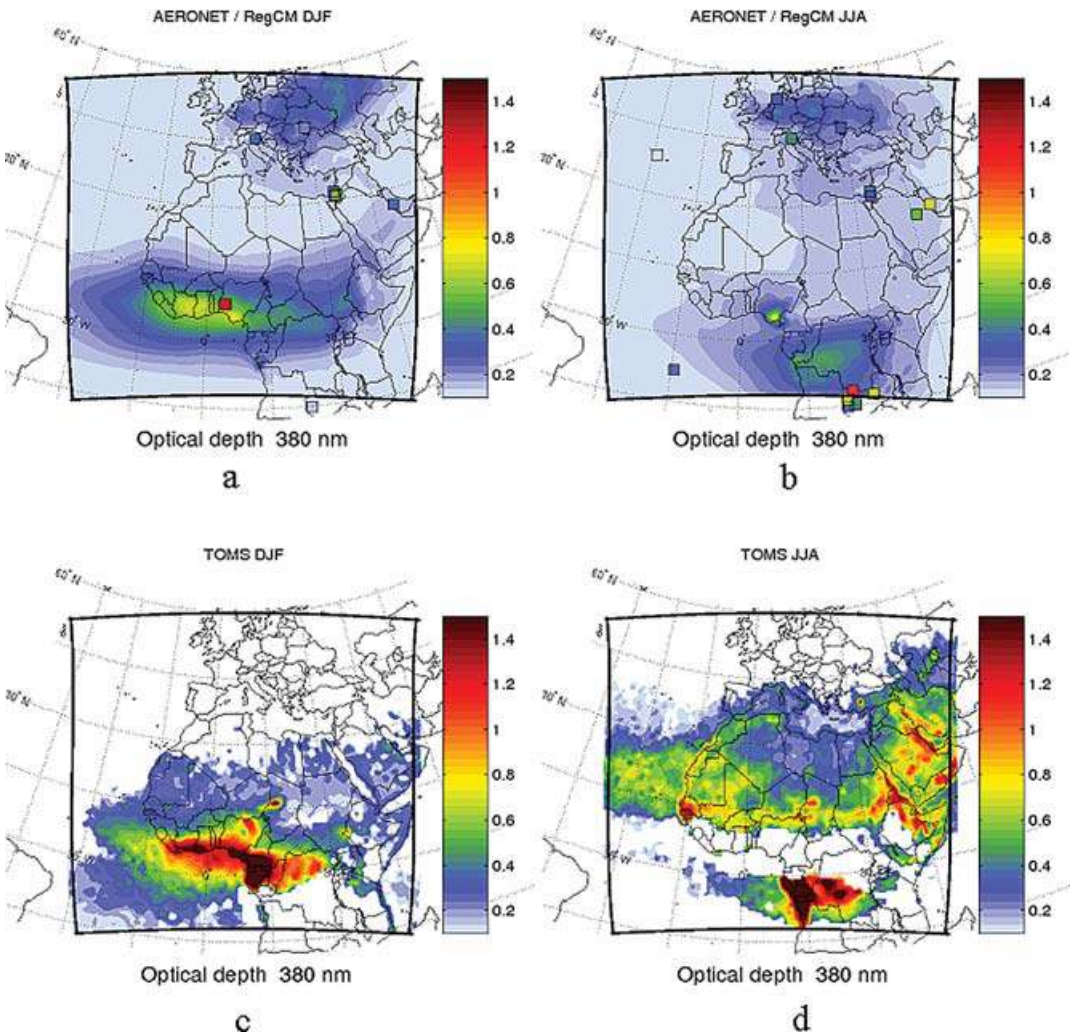

Fig 8. (a) Simulated AOD at 380 nm compared with averaged AERONET AOD measurements (coloured squares) for DJF. (b) Same as (a) but for JJA. (c) TOMS AOD retrieval (at 380 nm) for DJF 2000 (the white areas indicate no data availability).(d) Same as (c) but for JJA 2000.

sea although a model underestimation still remains. This underestimation (compared to MODIS AOD) and the above mentioned larger bias found in summer (compared to AERONET and MISR) are in line with the seasonal surface concentration underestimation of sulphate and carbonaceous compounds, as pointed out and discussed in Section 3.2. Finally, the lack of marine aerosol marine could also contribute in this model AOD underestimation over Mediterranean basin.

3.3.3. Africa. Over Africa, the AOD follows the dry season patterns: in DJF, maximum AOD is found over West Africa (between 0 and 15 N), while in JJA the AOD is maximum between 0 and 15 S. Despite a relatively low extinction coefficient considered in our calculations, OC is the main contributor to the optical depth (Fig. 6). Over highly urbanized regions (e.g. Lagos), the sulphate production can also be significant in enhancing the AOD (Figs. 7b and 8b). Because most aerosols are emitted in the dry season, the particle hygroscopic growth is limited close to the intense sources, but it is enhanced as we move closer to the coasts and over the sea.

In DJF, the comparison with the three West African AERONET stations shows an underestimation of the modelled AOD (Fig. 7a). In particular, over the Ilorin station (Nigeria) the observed AOD are more than twice the simulated values at 550 nm (less at 380 nm). Note, however, that the mean standard deviation associated with the AERONET measurements provided for these stations is quite high, ranging from 0.17 to 0.6 at Ilorin ($\sim$60% of the mea value). The same underestimation bias is obtained when comparing regionally the model and TOMS AOD (Figs. 8a and c). Part of the underestimation is due to Sahara and Sahelian dust particles emitted over dry surfaces and/or advected by the Harmattan. Despite these discrepancies in AOD magnitude, the spatial patterns corresponding to the biomass burning plume (eastern to 5 E and over the ocean) are consistent with the TOMS and AERONET observations.

The maximum of AOD observed over Cameroon and Gabon, where the dust contribution is likely weak, is not captured by the model. This maximum also appears in the TOMS 30 yearly AOD climatology (Torres et al., 2002), suggesting a systematic emission bias rather than an effect of the interannual variability of biomass burning emissions. Nevertheless, Torres et al. (2002) outline the sensitivity of TOMS AOD retrieval to the aerosol height assumptions, which can also potentially lead to a bias in satellite AOD retrievals over the mountainous regions of Africa In JJA the dust associated with African easterly waves (Jones et al., 2003) is likely to be a major component of the AERONET AOD measurement over the western Sahel. The dust contribution is particularly evident in the MISR and TOMS data (Figs. 7d and 8d) and mainly explains the model underestimation between 10 N and 20 N.

Over the biomass burning region (0–10 S), the model captures the spatial AOD pattern identified in the MODIS and MISR AOD. However, we still find a severe model underestimation of AOD. Over land, the MODIS seasonal AOD can reach values close to one, while the maximum value given by the model is about 0.35 (Figs. 7b and d). Some studies identified a positive bias of the MODIS AOD over land, and the MISR AODs are indeed lower (although still higher than the model AOD). Over ocean (south of the Guinea Gulf), the model reproduces the spatial extension of the plume and the discrepancies with the MODIS AOD are less pronounced. The same tendencies are also obtained at 380 nm when comparing the simulated AOD with the TOMS AOD (Figs. 8a–d). Such bias has also been found in other modelling studies (Reddy and Boucher, 2004; Stier et al., 2005; Penner et al., 2002; Liousse et al., 1997), which suggest that this underestimation may be attributed at least partially to uncertainties in biomass burning and fossil fuel sources. For instance, Chin et al. (2002) obtain higher AOD over biomass burning region, but using an emission inventory on an average 1.7–2 times higher than the inventory considered in this study. Beside emissions, uncertainties in smoke (specially the OC component) hygroscopic state and optical properties contribute to the model/satellite discrepancies. For instance Koch (2001) used a dry extinction coefficient of 8 m^2 g^{-1} for OC which would have in our case almost doubled the simulated values of AOD over Africa. At last, part of the AOD underestimation in JJA results from biomass burning sources situated beyond the southern limit of the domain and unaccounted for by the aerosol boundary conditions.

4. Sensitivity experiments

From Section 2, it can be seen that our model formulation depends on a number of critical assumptions and parameters. It is beyond the purpose of this paper to evaluate the model sensitivity to all of them. Therefore, we chose some illustrative cases, and more specifically we tested the model sensitivity to carbonaceous particles ageing parameter, European sulphur emission and convective transport. The discussion is limited to those variables analysed in the validation process above (AOD and surface concentrations).

4.1. Sensitivity to carbonaceous aerosol ageing constant

Here, we examine the impact of doubling the ageing time of carbonaceous aerosols, τ_{ag}, from 1.15 to 2.3 d. The resulting effect is an overall increase of the particle lifetime and an increase of aerosol amounts throughout the domain: the total burden of BC shows an increase of 9.5% in DJF and 10.7% in JJA, while for OC the increase reaches 5.6% in DJF and 7.2% in JJA. The difference between the impact on OC and BC is explained by the different hydrophobic/hydrophilic ratio considered at the emission. BC is more sensitive to τ_{ag} as it is mainly hydrophobic at the emission. The increase in BC burden over the domain is in between the results obtained by Cooke et al. (2002) and Reddy and Boucher (2004), who carried out similar sensitivity experiments. For OC, the increase in burden is a bit lower than in Reddy and Boucher (2004), who simulated a 10% increase.

In term of total optical depth, Figs. 9a and b illustrate the total AOD increase resulting from doubling the ageing parameter. The AOD difference reaches 0.03–0.04 over the Gulf of Guinea coastal regions in JJA and coincides with the location of maximum AOD. The corresponding relative AOD increase is 8–10% (Fig. 9c). A maximum relative AOD increase of about 35% is found slightly south of the equator over Congo (Fig. 9c). It results from the contributions of upwind sources to the north and the local high wet removal areas linked to the rainfall patterns. Increasing the ageing of particles allows them to penetrate further into the wet zone. We can also note a relative AOD increase over the ocean in direct link with the enhanced lifetime of easterly advected particles. The same kind of observations can be made for JJA, where the maximum AOD increase occurs in areas of maximum AOD (Fig. 9b), and the maximum relative AOD increase is found in the areas north of the precipitation band (Figs. 9d and 2). Over Europe, the impact of ageing on the total AOD is much lower since the total AOD is dominated by sulphates. Because of the more intense circulations during the winter season, the effect of the ageing parameter τ_{ag} on the AOD is greater in winter than in summer downwind of the source areas (Figs. 9c and d).

4.2. Sensitivity of SO_2 inventory over Europe

We present here a comparison of AOD obtained considering the EMEP and EDGAR databases as primary SO_2 emission inventories, respectively. Figures 10a and b show that the EDGAR database yields significantly higher AOD than the EMEP database. On an average, over the northern half of the domain (i.e. influenced by European emissions), the AOD values calculated from EDGAR are a factor of about 1.6 and 2 higher than those calculated from EMEP in DJF and JJA, respectively.

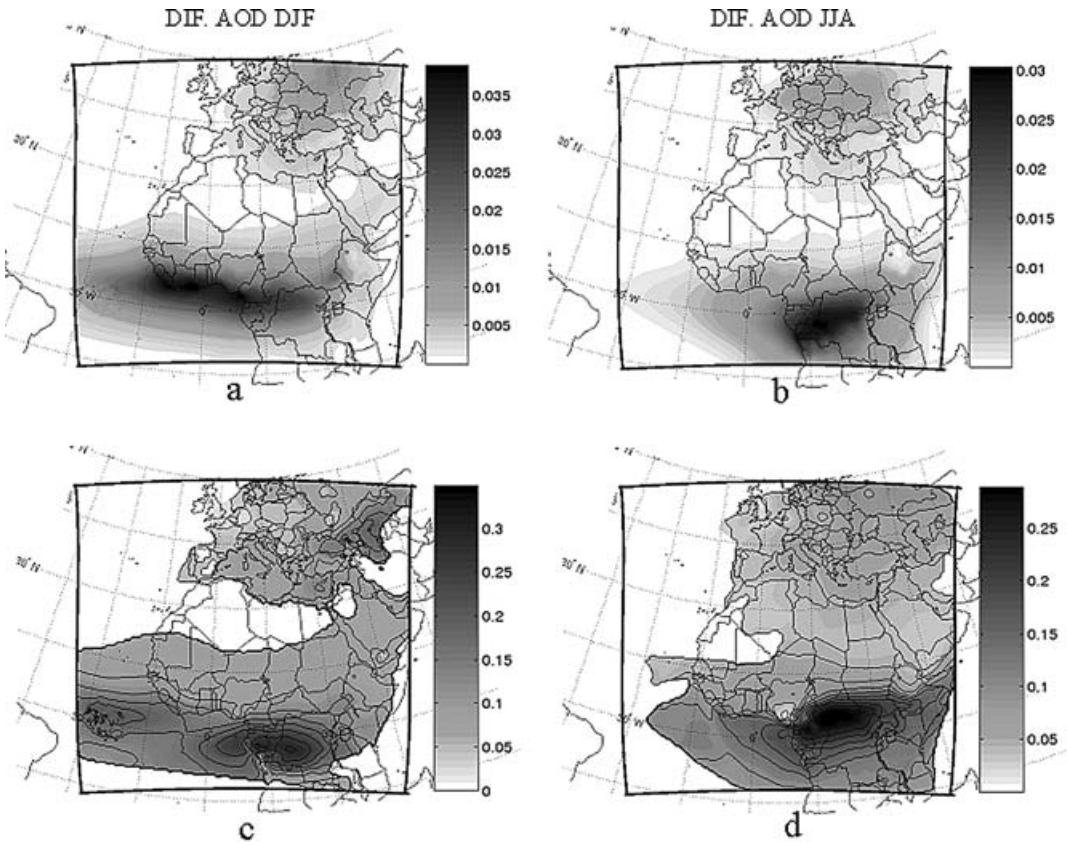

Fig 9. Sensitivity of AOD to the carbonaceous particle ageing. (a) AOD difference between a simulation using an ageing constant of 2.3 d ($\tau_{2.3}$) and a simulation using an ageing constant of 1.15 d ($\tau_{1.15}$) for DJF. (b) Same as (a) but for JJA. (c) Relative difference between the two cases calculated as $(\tau_{2.3} - \tau_{1.15})/\tau_{1.15}$ (restricted to significant values of AOD) for DJF. (e) Same as (c) but for JJA.

The lower increase factors obtained for DJF are partly due to the fact that more sulphate is lost through the northern boundary of the domain compared to JJA.

This average AOD difference when using the two emission datasets is close to linear with the emission flux differences between the inventories, the EDGAR emissions being roughly twice as intense as the EMEP emissions (Jeuken et al., 2001). In fact, the sulphate burden responds quasi-linearly to the SO_2 emissions. This result was also found by Qian et al. (2001) over east Asia and emphasizes the critical role of emission estimations with regards to aerosol uncertainties. Finally, Fig. 10 shows that changes in European emissions affect the AOD over the Mediterranean basin, particularly in summer when northerly advection and dry conditions favour the long-range transport of sulphates.

4.3. Sensitivity to convective transport

Vertical transport by deep cumulus convection can be very important especially in the summer season, and can efficiently carry the tracers from the boundary layer to the upper troposphere. As described in Section 2, when convection occurs, the tracer is simply mixed between the bottom and top convective levels. In order to test the influence of this simple hypothesis, we carried out a first-order test where this transport term was turned off. Differences in AOD obtained in this experiment are compared to the baseline case for JJA are shown in Figs. 11a and b.

Removal of the convective mixing tends to concentrate the aerosol amounts in the lowest layer of the atmosphere and decrease the concentrations in the mid to upper troposphere. This in turn affects the horizontal distribution of burdens and AOD. Particularly over Africa, there is a strong vertical shear between the low-level southwesterly monsoon flux and the northeasterly synoptic wind at the upper levels. Downwind of the Monsoon flux, the inhibition of the convective mixing induces an increase of AOD (Fig. 11b) which can reach 0.16 close to the Lagos region (i.e. a relative increase of $\sim$20%). Conversely, the AOD decreases to the south and east of the emission regions (e.g. over the ocean Fig. 11a). This relative decrease is also more widespread because it is linked to long-range high-altitude transport.

Over Europe, the westerly advection increases with altitude and therefore removing the vertical convective mixing tends to increase the AOD downwind of the source regions (Fig. 11b). This increase can reach 0.04 over central Europe (about 10% compared to the baseline case). An east–west dipole structure

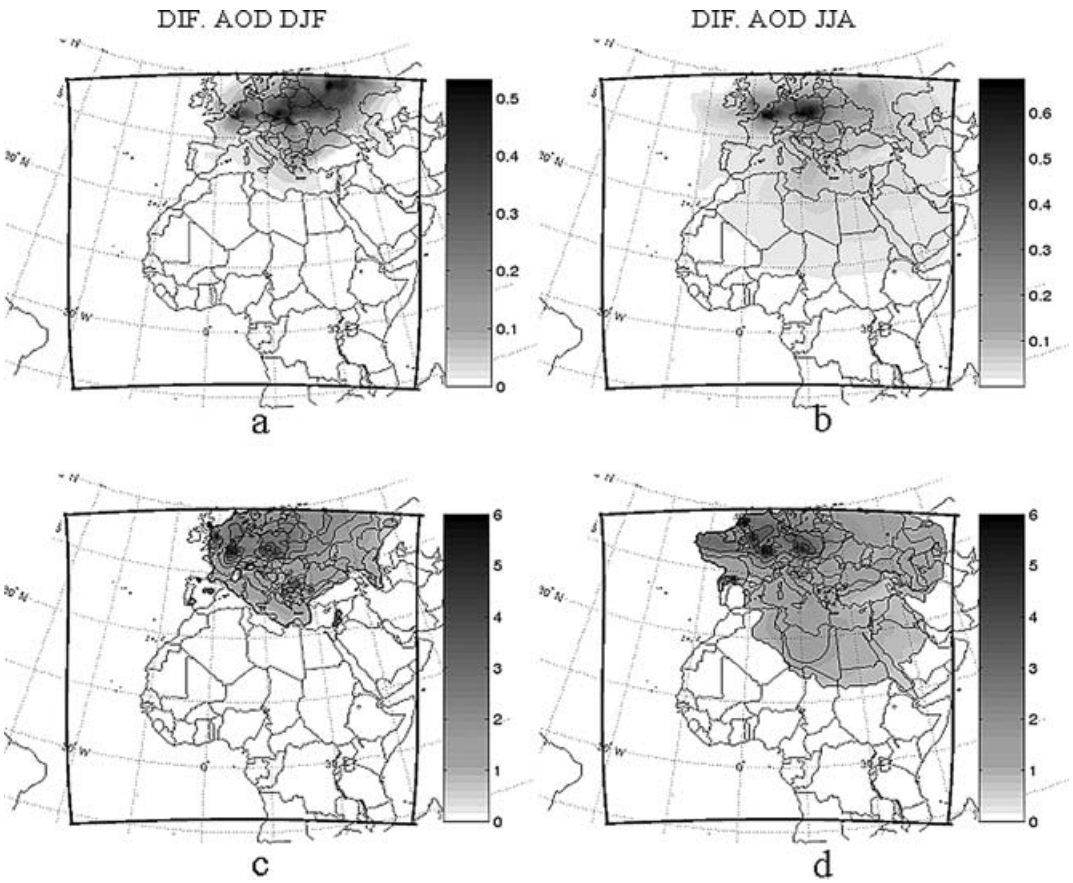

Fig 10. Sensitivity of AOD to SO_2 emission inventory. (a) AOD difference between a simulation including the EDGAR inventory and a simulation including the EMEP inventory over Europe for DJF. (b) Same as (a) but for JJA. (c) Corresponding relative differences calculated as (EDGAR−EMEP)/(EMEP) for DJF. (d) Same as (c) but for JJA.

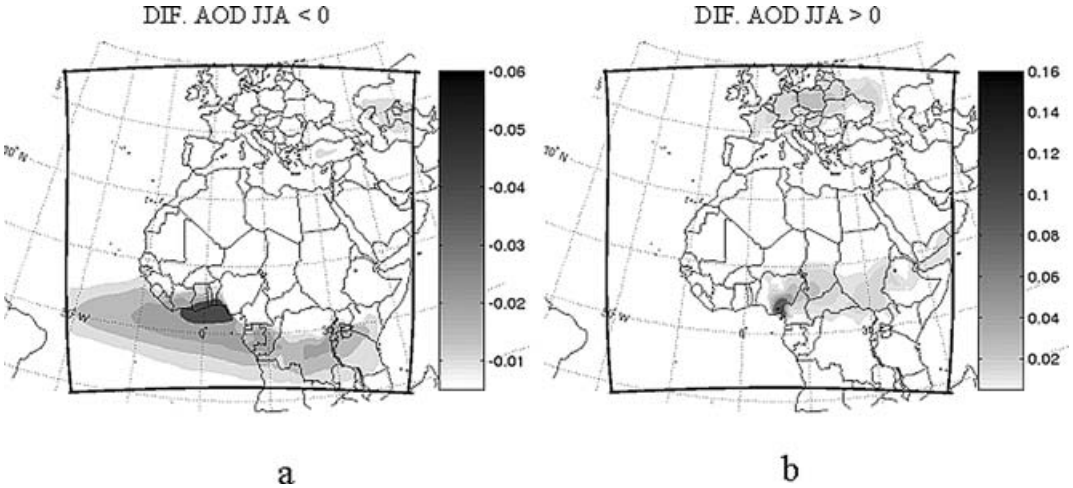

Fig 11. Sensitivity of AOD to the representation of deep convective transport. AOD differences between a simulation without convective transport and a simulation with convective transport (see text) for JJA. (a) Decrease of AOD when inhibiting the convection. (b) Increase of AOD when inhibiting the convection.

in the AOD change also appears over Europe although it is less pronounced than over Africa.

Over Europe, removing the convective transport induces a surface concentration increase ranging from +5 to +40% for SO_4^{2-} (+25% for OC and +20% for BC) in JJA. This tends to reduce the negative bias mentioned in Section 3.2. The biggest increase in surface concentration is found over equatorial Africa where this concentration can increase by a factor of 2.5 for OC and $SO4^{2-}$ and 1.4 for BC. It is therefore clear that uncertainties related to the representation of vertical convective transport can significantly affect the simulation of surface concentrations (Section 3).

5. Summary and conclusions

Simple model of anthropogenic aerosol, including the $SO2/SO_4^{2-}$ system, hydrophobic and hydrophilic BC and OC as well as their optical properties has been implemented within the RegCM regional model. An evaluation of the model performance was carried out over a wide and contrasted domain extending from northern Europe to southern sub-tropical Africa. Model results were confronted to various datasets of surface concentrations and AOD, both ground and remotely based, for the winter and summer 2000. Our main conclusions can be summarized as follows.

(i) The model reproduced the basic regional patterns and seasonality of anthropogenic aerosol over the domain. The comparison between simulated surface concentrations and EMEP measurements over Europe showed a statistically significant spatial correlation (correlation coefficients of 0.40 to 0.61). In 34 to 57% of cases, we found an agreement of sulphate surface concentrations with observations within a factor of 2. For OC and BC, more limited data were available. In this case, we found an agreement with observations within a factor of 2 in over 56% of cases (except for OC in JJA). Considering the uncertainties in the observation datasets, these results indicate a model performance comparable with that of previous, and in some cases more complex CTMs.

(ii) A general tendency shown by the model, both when looking at surface concentrations and AOD was to underestimate aerosol amounts, especially over the Mediterranean basin and in the summer season. Beside the uncertainties on primary sulphate OC and BC emissions, a number of reasons contribute to this bias. Foremost is the lack of natural aerosols, especially desert dust, biogenic secondary OC sources and anthropogenic nitrates. As shown by sensitivity experiments, the representation of vertical convective transport is also an important source of uncertainty, especially in warm climates. Moreover, assumptions in sulphate chemistry and wet deposition processes may also lead to an underestimate. We are addressing all these sources of uncertainty by including in our model additional natural aerosols (e.g. desert dust) and nitrates, and evaluating alternate vertical transport and wet removal schemes. This work will be reported in future papers.

(iii) A major problem over Africa is the lack of experimental data to develop accurate emission inventories and validate the models. For carbonaceous compounds (mainly emitted by biomass burning), simulated concentrations were close to the few available measurements. Simulated AOD over Africa showed consistency with observations in terms of spatial patterns but was underestimated in magnitude due to the lack of dust emissions (especially over the Sahel) and possibly underestimated primary emissions. In this regard, the current development of a new generation of inventories (Bond et al., 2004; Liousse et al., 2004; Generoso et al., 2003) is of great interest to test the model sensitivity to carbon emissions. Forthcoming experimental campaigns (e.g. the AMMA campaign) addressing these key issues should provide much needed information to validate the models.

As an overall summary assessment, the validation process shows that the regional model exhibits a performance in describing anthropogenic aerosol processes over this region at least comparable to other modelling efforts. The model is still currently not ready for application to climate change studies mostly because of the lack of some important natural aerosols (desert dust, marine and biogenic aerosols) and nitrates. Once this additional modelling effort is completed, we however assess that our modelling system can provide valuable information on the sensitivity of climate to anthropogenic aerosols in the European/African region.

6. Acknowledgments

We would like to acknowledge the EMEP, AERONET, MODIS, MISR and TOMS PI and their collaborators for building and providing an easy access to the diverse database used in this study. We thank also the two anonymous reviewers for their constructive critics.

References

Berner, A., Sidla, S., Galambos, Z., Kruisz, C. and Hitzenberger, R. 1996. Modal character of atmospheric black carbon size distributions. *J. Geophys. Res.* **101**, 19 559–19 565.

Bessagnet, B., Hodzic, A., Vautard, R., Beekmann, M., Cheinet, S. and co-authors. 2004. Aerosol modeling with CHIMERE- preliminary evaluation at the continental scale. *Atmos. Environ.* **38**, 2803–2817.

Bizjak, M., Tursic, J., Lesnjak, M. and Cegnar, T. 1999. Aerosol black carbon and ozone measurements at Mt. Krvavec EMEP GAW station, Slovenia. *Atmos. Environ.* **33**, 2783–2787.

Bond, T. C., Streets, D. G., Yarber, K. F., Nelson, S. M., Woo, J. H. and co-authors. 2004. A technology-based global inventory of black and organic carbon emissions from combustion. *J. Geophys. Res.* **109**, D14203, doi:10.1029/2003JD003697.

Cachier, H. 1998. Carbonaceous combustion Aerosols. In: *Atmospheric Particles* (eds. R. M. Harisson, and R. V. Van Grieken) pp. 296–323, John Willey and Sons Ltd, New York.

Cachier, H., Brémond, M. P. and Buat-Ménard, P. 1989. Determination of atmospheric soot carbon with a simple thermal method. *Tellus* **41B**, 379–390.

Cachier, H., Brémond, M. P. and Buat-Ménard, P. 1990. Organic and black carbon aerosols over marine regions of the Northern Hemisphere. In: *Proceedings of the International Conference on Global and Regional Environmental Atmospheric Chemistry* (eds. L. Newman et al), pp. 249–261, Dept. of Energy, Brookhaven Natl. Lab., Upton, NY.

Cachier, H., Sarda-Esteve, R., Oikonomou, K., Sciare, J., Bonazza, A. and co-authors. 2004. Aerosol characterization and sources in different European urban atmospheres: Paris, Seville, Florence and Milan.

Castro, L. M., Pio, C. A., Harrison, R. M. and Smith, D. J. T. 1999. Carbonaceous aerosol in urban and rural European atmospheres: estimation of secondary organic carbon concentrations. *Atmos. Environ.* **33**, 2771–2781.

Chameides, W. L. 1984. The photochemistry of a remote marine stratiform cloud. *J. Geophys. Res.* **89**, 4739–4755.

Chin, M., Ginoux, P., Kinne, S., Torres, O., Holben, B. N. and co-authors. 2002. Tropospheric aerosol optical thickness from the GOCART model and comparisons with satellite sunphotometer measurements. *J. Atmos. Sci.* **59**, 461–483.

Chung, S. H. and Seinfeld, J. H. 2002. Global distribution and climate forcing of carbonaceous aerosols. *J. Geophys. Res.* **107**, D194407, doi:10.1029/2001JD001397.

Cooke, W. F., Liousse, C., Cachier, H. and Feichter, J. 1999. Construction of a $1^\circ \times 1^\circ$ degree fossil fuel emission data set for carbonaceous aerosol and implementation and radiative impact in the ECHAM4 model. *J. Geophys. Res.* **104**, 22 137–22 162.

Cooke, W. F., Ramaswamy, V. and Kasibhatla, P. 2002. A general circulation model study of the global carbonaceous aerosol distribution. *J. Geophys. Res.* **107**(D16), 4279, doi:10.1029/2001JD001274.

Cubasch, U., Meehl, G. A., Boer, G. J., Stouffer, R. J., Dix, M. and co-authors. 2001. Projections of future climate change. In: *Chapter 9 of Climate Change 2001; The Scientific Basis, Contribution of Working Group I to the Third Assessment Report of the Intergovernmental Panel on Climate Change (IPCC)* (eds. J. T. Houghton, Y. Ding, D. J. Griggs, M. Noguer, P. J. van der Linden, and D. Xiaoxu) Cambridge University Press, Cambridge, UK, pp. 525–582.

Dickinson, R., Henderson-Sellers, A. and Kennedy, P. 1993. Biosphere–atmosphere transfer scheme (BATS) version 1e as coupled to the NCAR community climate model. Technical Report NCAR/TN-387 + STR, NCAR Boulder, Colorado.

Duncan, B., Portman, D., Bey, I. and Spivakovsky, C. 2000. Parameterization of OH for efficient computation in chemical tracer models. *J. Geophys. Res.* **105**, 12 259–12 262.

Dzubay, T. G., Stevens, R. K. and Haagenson, P. L. 1984. Composition and origins of aerosol at a forested mountain in Soviet Georgia. *Environ. Sci. Technol.* **18**, 873–883.

Ekman, A. M. L. and Rodhe, H. 2003. Regional temperature response due to indirect sulfate aerosol forcing: impact of model resolution. *Clim. Dyn.* **21**, 1–10.

Galy-Lacaux, C., Liousse, C., Guillaume, B., Rosset, R., Gardrat, E. and co-authors. 2004. Carbonaceous aerosols at the elevation site Pic du Midi (Pyrénées, France). *7eme International conference on carbonaceous aerosols*, *Vienna*, *14–16 of September*.

Generoso, S., Breon, F. M., Balkanski, Y., Boucher, O. and Schulz, M. 2003. Improving the seasonal cycle and interannual variations of biomass burning aerosol sources. *Atmos. Chem. Phys. Discuss.* **3**, 1973–1989.

Giorgi, F. 1989. Two-dimensional simulations of possible mesoscale effects of nuclear war fires. I: model description. *J. Geophys. Res.* **94**, 1127–1144.

Giorgi, F. and Chameides, W. L. 1986. Rainout lifetimes of highly soluble aerosols and gases as inferred from simulations with a general circulation model. *J. Geophys. Res.* **91**, 14 367–14 376.

Giorgi, F., Marinucci, M. R. and Bates, G. T. 1993a. Development of a second generation regional climate model (RegCM2). Part I: boundary-layer and radiative transfer processes. *Mon. Weather Rev.* **121**, 2794–2813.

Giorgi, F., Marinucci, M. R., Bates, G. T. and De Canio, G. 1993b. Development of a second generation regional climate model(RegCM2). Part II: convective processes and assimilation of lateral boundary conditions. *Mon. Weather Rev.* **121**, 2814–2832.

Giorgi, F. and Mearns, L. O. 1999. Introduction to special section: regional climate modeling revisited. *J. Geophys. Res.* **104**, 6335–6352.

Giorgi, F., Bi, X. and Qian, Y. 2002. Direct radiative forcing and regional climatic effects of anthropogenic aerosols over east Asia: a regional coupled climate-chemistry/aerosol model study. *J. Geophys. Res.* **107**, no. d16, 10.1029/2001JD001274.

Giorgi, F., Bi, X. and Qian, Y. 2003. Indirect versus direct effects of anthropogenic sulfate on the climate of east Asia as simulated with a regional coupled climate-chemistry/aerosol model. *Clim. Change* **58**, 345–376.

Grell, G. A. 1993. Prognostic evaluation of assumptions used by cumulus parameterizations. *Mon. Weather Rev.* **121**, 764–787.

Grell, G. A., Dudhia, J. and Stauffer, D. R. 1994. A description of the fifth-generation Penn State-NCAR Mesoscale Model (MM5). NCAR Tech. Note NCAR/TN-398+STR, National Center for Atmospheric Research, Boulder, Colorado, 122.

Haywood, J. M. and Boucher, O. 2000. Estimates of the direct and indirect radiative forcing due to tropospheric aerosols: a review. *Rev. Geophys.* **38**, 513–543.

Heintzenberg, J., Müller, K., Birmili, W., Spindler, G. and Wiedensohler, A. 1998. Mass-related aerosol properties over the Leipzig basin. *J. Geophys. Res.* **103**, 13 125–13 135.

Hitzenberger, R., Berner, A., Giebl, H., Koch, R., Larson, S. M. and co-authors. 1999. Contribution of carbonaceous material to cloud condensation nuclei concentrations in European background (Mt. Sonnblick) and urban (Vienna) aerosols. *Atmos. Environ.* **33**, 2647–2659.

Holben, B. N., Eck, T. F., Slutsker, I., Tanré, D., Buis, J. P. and co-authors. 1998. AERONET-A federated instrument network and data archive for aerosol characterization. *Remote Sens. Environ.* **66**, 1–16.

Holtslag, A. A. M., de Bruijin, E. I. F. and Pan, H. L. 1990. A high resolution air mass transformation model for short-range weather forecasting. *Mon. Weather Rev.* **118**, 1561–1575.

Ichoku, C., Kaufman, Y. J., Remer, L. A. and Levy, R. 2004. Global aerosol remote sensing from MODIS. *Adv. Space Res.* **34**, 820–827.

Janssen, N. A. H., VanMansom, D. F. M., VanDerJagt, K., Harssema, H. and Hoek, G. 1997. Mass concentration and elemental composition of airborne particulate matter at street and background locations. *Atmos. Environ.* **31**, 1185–1193.

Jeuken, A., Veefkind, P., Dentener, F., Metzger, S. and Robles Gonzalez, C. 2001. Simulation of the aerosol optical depth over Europe for August 1997 and a comparison with observations. *J. Geophys. Res.* **106**, 28 295–28 311.

Jones, C., Mahowald, N. and Luo, C. 2003. The role of easterly waves in African desert dust transport. *J. Clim.* **16**, 3617–3628.

Kalnay, M., Kanamitsu, M., Kistler, R., Collins, W., Deaven, D. and co-authors. 1996. The NCEP/NCAR 40-yr re-analysis project. *Bull. Am. Meteorol. Soc.* **77**, 437–471.

Kasibhatla, P., Chameides, W. L. and St. John, J. 1997. A three-dimensional global model investigation of seasonal variation in the atmospheric burden of anthropogenic sulfate aerosols. *J. Geophys. Res.* **102**, 3737–3759.

Kasten, F. 1969. Visibility in the prephase of condensation. *Tellus* **21**, 631–635.

Kaufman, Y. J., Tanré, D., Gordon, H., Nakajima, T., Lenoble and co-authors. 1997. Passive remote sensing of tropospheric aerosol and atmospheric correction for the aerosol effect. *J. Geophys. Res.* **102**, 16 815–16 830.

Kiehl, J. T., Hack, J. J., Bonan, G. B., Boville, B. A., Briegleb, B. P. and co-authors. 1996. Description of the NCAR Community Climate Model (CCM3). NCAR Technical Note, NCAR/TN-420+STR, 152.

Kiehl, J. T., Schneider, T. L., Rasch, P. J., Barth, M. C. and Wong, J. 2000. Radiative forcing due to sulfate aerosols from simulations with the National Center for Atmospheric Research Community Climate Model Version 3. *J. Geophys. Res.* **105**, 1441–1457.

Koch, D. 2001. The transport and direct forcing of carbonaceous and sulfate aerosols in the GISS GCM. *J. Geophys. Res.* **106**, 20 311–20 332.

Lelieveld, J., Berresheim, H., Borrmann, S., Crutzen, P. J., !Dentener, F. J. and co-authors. 2002. Global air pollution crossroads over the Mediterranean. *Science* **298**, 794–799.

Liousse, C., Dulac, F., Cachier, H. and Tanre, D. 1997. Remote sensing of carbonaceous aerosol production by African Savanna biomass burning. *J. Geophys. Res.* **102**, 5895–5911.

Liousse, C., Penner, J. E., Chuang, C., Walton, J. J., Eddleman, H. and co-authors. 1996. A global three-dimensional model study of carbonaceous aerosols. *J. Geophys. Res. Atmos.* **101**, 19 411–19 432.

Liousse, C., Andreae, M. O., Artaxo, P., Barbosa, P., Cachier, H. and co-authors. 2004. Deriving global quantitative estimates for spatial and temporal distributions of biomass burning emissions. In: *Emissions of Atmospheric Trace Compounds* (eds. C. Granier, P. Artaxo, and C. Reeves) Kluwer Academic Publishers, Dordrecht, The Netherlands, pp. 544.

Mallet, M., Roger, J. C., Despiau, S., Dubovik, P. and Putaud, J. P. 2003. Microphyscial and optical properties of aerosol particles in urban zone during ESCOMPTE. *Atmos. Res.* **69**, 73–97.

Martonchik, J. V., Diner, D. J., Kahn, R., Ackerman, T. P., Verstraete, M. M. Pinty, B. and Gorbon, H. R. and co-authors. 1998. Techniques for the retrieval of aerosol properties over land and ocean using multiangle imaging. *IEEE Trans. Geosci. Remote Sens.* **36**, 1212–1227.

Mätzler, C. 2002. MATLAB functions for Mie scattering and absorption. *IAP Res. Rep.* No. 02–08.

Menon, S., Hansen, J., Nazarenko, L. and Luo, Y. 2002. Climate effects of black carbon aerosols in China and India. *Science* **27**, 297: 2250–2253.

Molnár, A., Mészáros, E., Hansson, H. C., Karlsson, H., Gelencsér, A. and co-authors. 1999. The importance of organic and elemental carbon in the fine atmospheric aerosol particles. *Atmos. Environ.*, **33**, 2745–2750.

Myhre, G., Stordal, F., Johnsrud, M., Ignatov, A., Mishchenko, M. I. and co-authors. 2004. Intercomparison of satellite retrieved aerosol optical depth over the ocean. *J. Atmos. Sci.* **61**, 499–513.

Nunes, T. V. and Pio, C. A. 1993. Carbonaceous aerosols in industrial and coastal atmospheres. *Atmos. Environ.* **27**, 1339–1346.

Olivier, J. G. J., Berdowski, J. J. M., Peters, J. A., Bakker, J., Visschedijk, A. J. H. and and co-authors. 2001. Applications of EDGAR. Including a description of EDGAR 3.0: reference database with trend data for 1970–1995. RIVM, Bilthoven. RIVM report no. 773301 001/NOP report no. 410200 051.

Pal, J. S., Small, E. E. and Eltahir, E. A. B. 2000. Simulation of regional – scale water and energy budgets: Representation of subgrid cloud and precipitation processes within RegCM. *J. Geophys. Res.* **105**, 29 579–29 594.

Penner, J. E., Andreae, M., Annegarn, H., Barrie, L., Feichter, J. and co-authors. 2001. Aerosols, their direct and indirect effects. In: *Chapter 5 of Climate Change 2001; The Scientific Basis, Contribution of Working Group I to the Third Assessment Report of the Intergovernmental Panel on Climate Change (IPCC))*. (eds. J. T. Houghton, Y. Ding, D. J. Griggs, M. Noguer, P. J. van der Linden, and D. Xiaoxu) Cambridge University Press, Cambridge, UK, pp. 289–348.

Penner, J. E., Zhang, S. Y., Chin, M., Chuang, C. C., Feichter, J. and co-authors. 2002. A comparison of model- and satellite-derived aerosol optical depth and reflectivity. *J. Atmos. Sci.* **59**, 441–460.

Pio, C. A., Castro, L. M., Cequeira, M. A., Santos, I. M., Belchior, F. and co-authors. 1996. Source assessment of particulate air pollutants measured at the southern European coast. *Atmos. Environ.* **30**, 3309–332.

Putaud, J.-P., Baltensperger, U., Bruggemann, E., Facchini, M. C., Fuzzi, S. and co-authors. 2003. A European aerosol phenomenology. Physical and chemical characteristics of particulate matter at kerbside, urban, rural and background sites in Europe, Joint Research Centre, European Commission, EUR 20411 EN.

Qian, Y., Giorgi, F., Huang, Y., Chameides, W. L. and Luo, C. 2001. Simulation of anthropogenic sulphur over east Asia with a regional coupled chemistry-climate model. *Tellus* **53B**, 171–191.

Qian, Y., Leung, L. R., Ghan, S. J. and Giorgi, F. 2003. Regional climate effects of aerosols over China: modeling and observations. *Tellus* **55B**, 914–934.

Reddy, M. S. and Boucher, O. 2004. A study of the global cycle of carbonaceous aerosols in the LMDZT general circulation model. *J. Geophys. Res.* **109**, D14202, doi:10.1029/2003JD004048.

Reid, J. S., Hobbs, P. V., Ferek, R. J., Blake, D. R., Martins, J. V. and co-authors. 1998. Physical, chemical, and optical properties of regional hazes dominated by smoke in Brazil. *J. Geophys. Res.* **103**, 32 059–32 080.

Reid, N., Misra, P. K., Bloxam, R., Yap, D., Rao, S. T. and co-authors. 2001. Do we understand trends in atmospheric sulphur species. *J. Air Waste Manage. Assoc.* **51**, 1561–1567.

Reid, J. S., Eck, T. F., Christopher, S. A., Koppmann, R., Dubovik, O. and co-authors. 2004. A review of biomass burning emissions part III: intensive optical properties of biomass burning particles. *Atmos. Chem. Phys. Discuss.* **5**, 827–849.

Riemer, N., Vogel, H. and Vogel, B. 2004. Soot aging time scales in polluted regions during day and night. *Atmos. Chem. Phys.* **4**, 1885–1893.

Roelofs, G. J., Kasibhatla, P., Barrie, L., Bergmann, D., Bridgeman, C., and co-authors. 2001. Analysis of regional budgets of sulphur species modelled for the COSAM exercise. *Tellus* **53B**, 673–694.

Ruellan, S., Cachier, H., Gaudichet, A., Masclet, P. and Lacaux, J. P. 1999. Airborne aerosols over central Africa during the experiment for regional sources and sinks of oxidants (EXPRESSO). *J. Geophys. Res.* **104**, 30 673–30 690.

Schaap, M., vanLoon, M., ten Brink, H. M., Dentener, F. J. and Builtjes, P. J. H. 2003. The nitrate aerosol field oer Europe: simulations with an atmospheric chemistry-transport model of intermediate complexity. *Atmos. Chem. Phys. Discuss* **3**, 5919–5976.

Seigneur, C. 2001. Current status of air quality model for particulate matter. *J. Air Waste Manage. Assoc.* **51**, 1508–1521.

Seinfeld, J. and Pandis, S. N. 1998. *Atmospheric Chemistry and Physics.* John Wiley and Sons Inc., New York.

Smith, D. J. T., Harrison, R. M., Luhana, L., Pio, C. A., Castro, L. M. and co-authors. 1996. Concentrations of particulate airborne polycyclic aromatic hydrocarbons and metals collected in Lahore, Pakistan. *Atmos. Environ.* **30**, 4031–4040.

Stier, P., Feichter, J., Kinne, S., Kloster, S., Vignati, E. and co-authors. 2005. The aerosol-climate model ECHAM5-HAM. *Atmos. Chem. Phys. Discuss.* **5**, 1125–1156.

Tan, Q., Huang, Y. and Chameides, W. L. 2002. Budget and export of anthropogenic SOx from east Asia during continental outflow conditions. *J. Geophys. Res.* **107**(D13), 4167, doi:10.1029/2001JD000769.

Tanré, D., Remer, L. A., Kaufman, Y. J., Mattoo, S., Hobbs, P. V. and co-authors. 1999. Retrieval of aerosol optical thickness and size distribution over ocean from the MODIS airborne simulator during TARFOX. *J. Geophys. Res.* **104**, 2261–2278.

Torres, O., Bhartia, P. K., Herman, J. R. and Ahmad, Z. 1998. Derivation of aerosol properties from satellite measurements of backscattered ultraviolet radiation. Theoretical Basis. *J. Geophys. Res.* **103**, 17 099–17 110.

Torres, O., Bhartia, P. K., Herman, J. R., Sinyuk, A. and Holben, B. 2002. A long term record of aerosol optical thickness from TOMS observations and comparison to AERONET measurements. *J. Atmos. Sci.* **59**, 398–413.

Tsigaridis, K. and Kanakidou, M. 2003. Global modeling of secondary organic aerosol in the troposphere: a sensitivity analysis. *Atmos. Chem. Phys. Discuss.* **3**, 1849–1869.

van Loon, M., Roemer, M. G. M., Builtjes, P. J. H., Bessagnet, B., Rouil, L. and co-authors. 2004. Model inter-comparison. In the framework of the review of the Unified EMEP model. TNO-MEPO-R 2004/282. – TNO Report 282: 86 pp.

Vestreng, V. 2003. EMEP/MSC-W Technical report. Review and Revision. Emission data reported to CLRTAP. MSC-W Status Report 2003. EMEP/MSC-W Note 1/2003. ISSN 0804–2446.

Wolff, E. W. and Cachier, H. 1998. Concentrations and seasonal cycle of black carbon in aerosol at a coastal Antarctic station. *J. Geophys. Res.* **103**, 11 033–11 041.

Yaaqub, R. R., Davies, T. D., Jickells, T. D. and Miller, J. M. 1991. Trace-elements in daily collected aerosols at a site in southeast England. *Atmos. Environ.* **45A**, 985–996.

Zappoli, S., Andracchio, A., Fuzzi, S., Facchini, M. C., Gelencsér, A. and co-authors. 1999. Inorganic, organic, and macromolecular components of fine aerosols in different areas of Europe in relation to their water solubility. *Atmos. Environ.* **33**, 2733–2743.